Sustainable Energy, Grids and Networks 41 (2025) 101601

Contents lists available at ScienceDirect

Sustainable Energy, Grids and Networks

journal homepage: www.elsevier.com/locate/segan

Enhancing voltage optimization in distribution networks through flexible operation of EV parking lots ☆

Michele De Santis [a,*], Tohid Harighi [b], Anna Rita Di Fazio [c], Alberto Borghetti [b], Mario Russo [c]

[a] University of Campania "Luigi Vanvitelli", Department of Engineering, via Roma, 9, Aversa 81031, Italy
[b] University of Bologna, Department of Electrical Energy and Information Engineering, Viale del Risorgimento, 2, Bologna 40136, Italy
[c] University of Cassino and Southern Lazio, Department of Electrical and Information Engineering, via Gaetano di Biasio, 43, Cassino 03043, Italy

ARTICLE INFO

Keywords:
Electric vehicle aggregator
Energy recovery
Linear power flow
Power flexibility
Stochastic optimization
Voltage optimization problem

ABSTRACT

This study focuses on the use of consumption flexibility provided by a parking lot (PL) equipped with charging stations for electric vehicles to improve the voltage control in distribution networks. A methodology is presented in which PL offers both upward and downward flexibility of power consumption, provided that energy recovery is guaranteed in subsequent time intervals. To define the flexibility offered by the PL, the proposed approach uses a stochastic optimization model that computes the day-ahead absorption profiles and the maximum allowable flexibility for each 15-minute interval, expressed in terms of the power adjustment capability of the PL in response to the distribution system operator (DSO) request. The DSO then optimizes the voltage profile of the distribution network using the power flexibility offered by the PLs, as well as by other distributed energy resources (DERs). A multiperiod horizon is used in the voltage optimization problem to account for the effects of energy recovery in subsequent intervals. The results are presented for simulations of 24-hour operation of the IEEE 123-node test feeder with four flexible PLs and 15 DERs, whose reactive powers can be varied. The results for two days show an improvement of approximately 70% in terms of voltage profiles in comparison with the case without any voltage optimization, with 30% of the specific contribution of PLs compared to only DERs optimization. The full recovery in terms of the energy provided by each PL is verified, and a cost analysis from the DSO perspective is presented.

1. Introduction

The concept of distribution system services (DSSs) is essential for innovative management schemes of distribution system operators (DSOs) in future flexible power systems [1]. The DSSs are necessary to cope with the uncertainties related to generation from renewable energy sources (RESs), such as photovoltaic (PV) systems, as well as to load consumption and network contingencies. The DSSs are provided by distributed energy resources (DERs), which include individual suppliers such as passive end-users participating in demand response programs, active end-users with local generators and/or storage units, and energy communities [2]. In this new paradigm, DERs are viewed as a flexible resource that supports network operation [3].

Another trend driven by environmental concerns is the transition from internal combustion vehicles to electric vehicles (EVs) [4]. The integration of EVs into conventional electric power systems presents several challenges that require the development of novel optimal planning approaches [5]. In addition, the random charging behavior of EVs can negatively affect the operation of the distribution system. On the other hand, if properly managed, EVs can become DERs that provide DSSs to the DSO [6]. A detailed review of the literature on this topic is available in [7]. EVs behave differently from conventional electrical loads because they store energy in their batteries and may exchange energy between them [8]. Then, appropriate management systems installed in parking lots (PLs) allow a control of the aggregated power required by the EVs, providing the flexibility service [9]. Also, the framework of energy communities can integrate the function of EV charging stations aggregation [10].

Among DSSs, this paper focuses on voltage profile optimization which concerns DSOs when a large number of charging EVs are connected to the distribution grid. Some other DSSs, such as frequency regulation, are wide area services that refer to wholesale markets

☆ This paper presents the results obtained in research activities funded by the Italian Ministry for University and Research through grant J35F21003140006 (Ph.D. program 2014IT16M2OP005), grant PRIN-20228E3T44 "Smart and/or sustainable mobility" and through MUR Decree n. 1051 23.06.2022 PNRR Missione 4 Componente 2 Investimento 1.5, Project ECS 0000024 "Ecosistema dell'innovazione - Rome Technopole" CUP H33C22000420001.

* Corresponding author.
E-mail address: michele.desantis@unicampania.it (M. De Santis).

https://doi.org/10.1016/j.segan.2024.101601
Received 30 May 2024; Received in revised form 9 November 2024; Accepted 9 December 2024
Available online 3 January 2025

Nomenclature

Δt	Single time period duration of 15 min
n_{rec}	Predefined number of subsequent intervals to recover the power change after a flexibility interval

PL flexibility model

ω	Scenario index
π^{ω}	Probability of scenario ω
$S_{\text{in}}^{\omega,t}$	Set of entering EVs for each scenario ω and time period t
$S_{\text{out}}^{\omega,t}$	Set of leaving EVs for each scenario ω and time period t
$E_{\text{S+}}^{\omega,t}$	Total energy stored in the EVs arriving in the parking lot at time t
$E_{\text{S-}}^{\omega,t}$	Total energy leaving the parking lot due to EV departures at time t
$E_{\text{S net}}^{\omega,t}$	Net energy stored by the EV batteries at the end of period t
$E_{\text{Smax}}^{\omega,t}$	Summation of the rated size of the EV batteries present in the parking lot in scenario ω at time t
$E_{\text{ini},j}^{\omega,t}$	Initial energy of the EVs arriving in period j and leaving in period t ($j = 0$ indicates that the relevant EVs are already parked when the optimization horizon begins)
$E_{\text{g},j}^{\omega,t}$	Total charge needed for EVs arriving in period j and leaving in period t (i.e., difference between the final charge and the initial charge)
$E_{\text{ch},j}^{\omega,t}$	Minimum energy profile that guarantee the adequate charging of the vehicles arriving in period j before leaving the parking lot
$P^{\omega,t}$	Power absorbed from the grid (limited by P_{max})
$P_{\text{max}}^{\omega,t}$	Sum of the maximum power of the EV charging stations in use at time t
$P_{\text{ref}}^{\omega,t}$	Reference consumption profile
$\Delta P_{\text{flex up}}^{\omega,t}$, $\Delta P_{\text{flex down}}^{\omega,t}$	Flexibility margins at time t
$C_{\text{S}}^{\omega,t}$	Cost of using of the initial energy stored in the vehicles
$W_{flex}^{\omega,t}$	Revenue associated with the provision of the maximum flexibility at time t
ρ_{TOU}^{t}	Time of use tariff for the purchase of energy from the grid, at time t
ρ_{μ}	Tariff for the use of the initial energy in the entering EVs
ρ_{flex}^{t}	Tariff for the provision of the flexibility service
$\mu^{\omega,t}$	Fraction of the initial energy used to ensure that a minimum energy margin e_{min} is maintained in the EV batteries at time t
η_{ch}	Efficiency of the EV batteries charging from the grid
δ	Battery self-discharge rate
$l_{\text{V2V}}^{\omega,t}$	Vehicle-to-vehicle charge transfer losses at time t
t_{flex}	Flexibility time period
n_{flex}^{+}	Additional consecutive period of flexibility

DSO voltage optimization model

PN	Pilot node
VCZ	Voltage control zone
P_{der}^{t}, Q_{der}^{t}	Variations of active and reactive power of DERs
P_{evpl}^{t}	Active power absorbed by the EV PL at time t
$P_{\text{flex up}}^{t}$, $P_{\text{flex down}}^{t}$	Upward and downward flexibility used at time t
b_{DSO}^{t}	Allocated budget of the DSO at time t for voltage regulation service
c_{pl}^{t}, c_{der}^{t}	Linear cost functions of PL and DER, respectively, at time t
Γ_{der}, Γ_{evpl}, Γ_{load}	Matrices of voltage sensitivity coefficients of DERs, EVPLs and loads, respectively
$\bar{R}_{\text{down}}^{n_{\text{rec}},t}$, $\bar{R}_{\text{up}}^{n_{\text{rec}},t}$	Active power recovered, at time t, for the up and down flexibilities used in the previous n_{rec} periods
$V_{\text{pn},i}^{t}$	PN Voltage of VCZ i at time t

operated by the transmission system operator, and the coordination between local and wholesale markets for ancillary services requires special attention [11]. This kind of DSSs are beyond the scope of this paper. Then, the aim of this paper is to present an optimization procedure of the voltage profile in distribution grids which exploits the flexibility offered by PL operators, aggregating and shifting the active powers absorbed by their EV charging stations.

1.1. Previous literature

Many investigations have explored voltage optimization in distribution systems exploiting the flexibility of DERs, including EVs, as reviewed in [12] and references therein. Recent studies can be categorized based on the methodologies employed, such as stochastic approach (e.g. Monte Carlo simulations), optimization schemes, and multi-objective strategies.

Among the stochastic approaches, in [13], a Monte Carlo simulation method is used to evaluate the impact of uncontrolled EV charging behavior on the voltage profiles. This study uses dynamic game theory to schedule EV charging to improve the network voltage profile. Several studies focus on the financial benefits and market participation of EV aggregators using economic and market-based models [14]. In [15], a bi-level model for PL participation to the energy, reserve, and regulation markets is proposed to ensure that technical constraints are met while costs are minimized. Similarly, [16] presents a framework for scheduling distribution companies with EV PLs and renewable energy sources, maximizing company profits by minimizing power purchase costs and optimizing PL owner profits. In [17] an operational model for distribution companies is presented to reduce costs by exploiting the flexibility of EV aggregators using linear decision rules and distributionally robust optimization to deal with uncertainties. In [18] a framework is outlined for optimal scheduling of EV charging and discharging based on transactive principles. In this system, the EV aggregators submit their day-ahead bids to the DSO, that resolves the day-ahead market by considering the bids of all prosumers and the load demand necessary to clear the market. Then the DSO determines the local marginal price for the distribution area, which are used as inputs to the charge–discharge scheduling optimization problem. Finally, other studies, such as [19], propose a day-ahead scheduling model that offers tariff discounts to PL operators. The adopted bi-level program aims to reduce the peak-off-peak power differences and the peak-to-average ratio and to improve flexibility, benefiting both DSOs and PL operators.

Regarding the optimization schemes, the research outlined in [20] introduces a technique to maximize the efficiency of short-term EV charging and discharging operations, taking into account the possible reduction of active power due to volt-var control, while giving priority to reactive power output. First, the aggregator provides the DSO with an optimized schedule to evaluate the expected active power curtailment through power flow analysis. Then, the aggregator modifies the active power output constraint to avoid the expected curtailment and performs a second optimization process for EV charging and discharging operations. The method proposed in [21] aims to satisfy EV owners by effectively controlling the EV charging for voltage management in a low-voltage distribution network. This is achieved through a dynamic curtailment approach that provides incentives to prioritize the preferences of EV owners. Through their home energy management systems, EV owners participate in the local energy market by submitting bids to the retail sector and making decisions regarding energy transactions. This voltage regulation method uses voltage sensitivity coefficients to influence EV energy transactions through a price-based market system. Similarly, in [22] the charge/discharge flexibility of EVs is exploited to address congestion and voltage issues within distribution networks. The concept of transactive energy allows participants to exchange energy within a local market through a bidding mechanism, taking into account their individual preferences and the limitations of the network infrastructure. Coordinating a large number of EVs proves to be an effective means of managing distribution systems, improving both control capabilities and computational efficiency. In [23], a convex optimization problem is presented to control the EV charging process, aiming at minimizing individual charging costs. The flexibility of this system is demonstrated by its ability to determine the optimal charging and discharging times based on both the vehicle battery state of charge and the distribution network operating condition. In [24] a two-stage control scheme is adopted with voltage support functions for PV generation and EVs. The day-ahead and intraday control stages aim to mitigate voltage deviations, with the intraday stage employing real-time rolling optimization. Adopting a centralized control approach, a method to integrate EV charging with on-load tap changer (OLTC) settings is presented in [25]. This method involves two steps: setting the voltage profile using the OLTC and calculating the consumption of the EVs to follow the predicted PV generation fluctuations. The computational effort is significant because the proposed approach requires solving two quadratic optimal power flows and a large-scale linear optimization problem.

Many studies have proposed multi-objective optimization strategies, such as minimizing voltage deviations, power losses, and total operating costs. In [5], a mixed-integer multi-objective optimization scheme is proposed to integrate and utilize EVs to improve the reliability of the distribution system. The objectives are to minimize the unsupplied energy and power losses while improving the voltage profile. In this study, a heuristic particle swarm optimization algorithm is used to determine the optimal PL locations and charging patterns over 24 h. Similarly, [26] presents a multi-objective reactive power optimization model using a dual-population-based evolutionary algorithm for high penetration scenarios of wind and PV generation and EVs. The proposed algorithm minimizes voltage deviations and power losses, although the paper is primarily focused on the algorithm performance rather than realistic modeling of EV behavior. In [27], the complex optimization challenge of harmonizing EV charging requirements with networks constraints is tackled through the application of the Meerkat optimization algorithm. The methodology simultaneously addresses the multi-objective optimization of various factors, including energy losses, power purchases, load reduction, costs associated with distributed generation, battery systems, and EV-related expenditures. In [28] a model for reconfiguring distribution networks is presented to accommodate new energy sources and EVs. The model is designed to determine the optimal configuration of tie switches and to develop a reactive power regulation strategy, using a new multi-objective optimization algorithm that focuses on minimizing line loss and voltage deviation as its primary objectives. The model considers the reactive power outputs of new energy sources and EVs as variables that can be controlled. In [29], a two-layer strategy is adopted for an energy management system at the low-voltage level. The first layer regulates EV scheduling and energy consumption, while the second layer minimizes voltage deviations and energy losses using heuristic multi-objective optimization. Finally, [30] formulates a collaborative EV charging scheduling and voltage control strategy based on deep reinforcement learning (DRL) to schedule EV charging and distribution network voltage control.

Table 1 summarizes the main features of the models and algorithms reported above with reference to the contribution that can be provided to distribution system management by controlling EV charging/discharging, together with other DERs.

1.2. Specific contribution

In the frame outlined in the previous subsection, this paper focuses on two main aspects. The first one concerns the evaluation of the maximum flexibility that PLs can offer to the DSO while guaranteeing the EV charging service. The second aspect is exploiting this flexibility, along with the one of other DERs, to optimize the network voltage profile in real time. Accordingly, two procedures are proposed. The first one focuses on the pre-calculation by each PL operator of the flexibility margins, i.e., how much the power consumption can be reduced or increased with respect to the forecasted reference profile, following a DSO request, while still guaranteeing the appropriate charging level of the parked EVs. Since the characteristics and the number of cars connected to the charging stations during the day are uncertain [31], the procedure applies a multi-stage stochastic optimization approach. The second procedure deals with the centralized optimization for voltage control in the distribution network, exploiting the flexibility margins offered by the PLs. The procedure is based on the solution of an on-line voltage optimization problem, in which the network is decomposed into voltage control zones (VCZs), each characterized by a pilot node (PN) (i.e., the node most representative of the operating conditions of the VCZ) [32,33].

The proposed methodology, which is an extension and generalization of the method first described in [34], introduces a stochastic procedure that implements a linear optimization model to compute the reference absorption profiles of the PLs and the maximum allowed increase or decrease in active power flexibility for every 15 min of each 6-h stage considered during the day. With respect to [34], this paper includes a more accurate representation and description of the parking lot flexibility service, including the ability to offer maximum power reduction and increase margins in consecutive 15-min periods. The profiles of the reference consumption and the up and down flexibility margins are provided to the DSO, which in turn performs a voltage optimization and determines the actual power variation request to be sent to the PL operators, as shown in Fig. 1. A multiperiod voltage optimization procedure is proposed, which is significantly improved with respect to [34], both on the logic of choosing the right interval to use PL flexibility and on the management of the energy recovery strategy. The implementation is now streamlined and faster than its first release [34], improving its voltage regulation performance and allowing its use in real-time applications.

As stated in [35], the challenge in providing flexibility through EVs is the need to schedule energy recovery under a strict deadline. To guarantee adequate charging service, the proposed procedure assumes a mutual understanding between the PL operators and the DSO, allowing the PL operator to adjust power within a predetermined recovery interval after the flexibility provision. Each flexibility margin is

Table 1
Comparison of previous contributions in the literature on the effects of EV charging on distribution networks classified according to the presence of the EV aggregator, i.e., Agg.: (yes if present, no if absent); the model, i.e., MS: multi-objective strategy (CMOP: constrained multi-objective optimization, MAS: multi-agent systems, MDP: Markov decision process, OED: optimal energy dispatch, ORPF: optimal reactive power flow, QP: quadratic programming); O: optimization scheme (CCP: chance-constrained programming, CP: convex programming, LP: linear programming, MILP: mixed integer linear programming, OPF: optimal power flow, ROPF: rolling optimization power flow); ST: stochastic approach (DG: dynamic game, LDR: linear decision rule, MC-RO: Monte Carlo robust optimization); the type of algorithm, i.e. D: deterministic (ADMM: alternating direction method of multipliers, CPLEX: commercially available optimization software package, FA: Floyd algorithm, PSD-CR: positive semidefinite convex relaxation, RO: robust optimization, SDA: scheduling dispatch algorithm, •: algorithm not specified); MH: metaheuristics (ARSBX: adaptive rotation-based simulated binary crossover, c-DPEA: dual-population-based evolutionary algorithm, DDPG: deep deterministic, JA: Jaya algorithm, MOA: meerkat optimization algorithm, MOGA: multiobjective genetic algorithm).

Literature review							
Reference	Agg.	Model			Algorithm		Objective
		MS	O	ST	D	MH	
[4]	Yes	MAS	–	–	•	–	Network limit fulfillment
[8]	No	–	LP	–	•	–	Peak-shaving & valley-filling control
[10]	No	–	CCP	–	ADMM	–	energy community day-ahead reserve
[12]	No	–	MILP	–	•	–	Minimizing energy net operating cost
[13]	No	–	–	DG	FA	–	Costs & revenues
[15]	Yes	–	–	LP	CPLEX	–	Overall cost minimization
[16]	Yes	–	–	MILP	CPLEX	–	Overall profit optimization
[17]	Yes	–	–	LDR	•	–	Cost optimization
[18]	Yes	–	–	MC-RO	•	–	Minimize costs & satisfy EV owner scheduling
[19]	No	–	–	MILP	CPLEX	–	Overall profit optimization
[20]	Yes	–	MILP	–	CPLEX	–	Maximize revenues & satisfy voltage constraints
[21]	No	–	QP	–	•	–	Maximize social welfare & satisfy voltage constraints
[22]	Yes	–	QP	–	•	–	Maximize social welfare & satisfy network constraints
[23]	No	–	CP	–	SDA	–	Minimize charging costs
[24]	No	–	ROPF	–	–	JA	Voltage regulation
[25]	No	–	OPF	–	PSD-CR	–	Improving network voltage profile
[26]	No	ORPF	–	–	–	c-DPEA	Line losses, voltage deviation & stability
[27]	No	QP	–	–	–	MOA	Minimize losses & overall costs
[28]	No	CMOP	–	–	–	ARSBX	Minimize voltage deviations & losses
[29]	Yes	OED	–	–	–	MOGA	Load flattening, voltage regulation & charging costs
[30]	No	MDP	–	–	–	DDPG	EV scheduling & voltage control

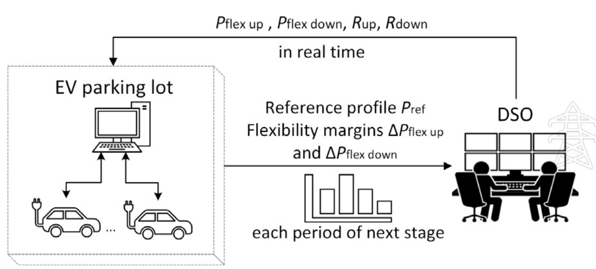

Fig. 1. Procedure scheme: At the beginning of each 6-h stage, the PL operator provides the DSO with reference power absorption profiles and the corresponding up and down flexibility margins. The DSO performs real-time voltage profile optimization and returns power change requests and energy recovery (either up or down) to the PL every 15 min.

therefore associated with an energy restoration of opposite sign within the recovery interval. Consequently, the voltage optimization problem accounts for the effects of the use of PL flexibility on the subsequent time intervals, through a multiperiod model.

Compared to the previous literature, the novelty of this study is threefold:

- An aggregator model is proposed in which each PL, through stochastic optimization of both costs and revenues, provides the DSO with the scheduled consumption profiles and the flexibility margins, assuming that the overall energy absorption is constant and the EV charging service is guaranteed by timely energy recovery.
- The consumption profiles and flexibility are used by the DSO, together with the flexibility provided by other DERs, to perform a deterministic optimization of the network voltage profile, based on a recently validated linear model [32] extended to the presence of PLs equipped with EV charging stations.
- The optimization is performed by the DSO with a multiperiod model, so that the PL flexibility is exploited while accounting for the effects of the energy recovery on the voltage profile in the subsequent periods.

The overall methodology, comprehensive task organization, and associated execution times are shown in Fig. 2. The maximum power reduction and increase margins of the parking lot were calculated in advance for the following day. The parking lot aggregator considers decisions based on shorter time horizons infeasible because they do not sufficiently consider future arrivals and departures. The uncertainty in forecasting EV arrivals and departures justifies the stochastic approach. A multi-stage linear programming procedure was implemented to adapt the flexibility margin decision during the day to the actual number of EVs present in the parking lot. The DSO optimizes the voltage by using the pre-calculated flexibility margins from the EV parking lot. This was repeated every 15 min, with a short optimization horizon for which the uncertainties associated with load consumption and DER production were considered negligible in this study.

The structure of the paper is the following. Section 2 describes the multi-stage stochastic optimization model of the PL to compute the reference consumption profile and the flexibility margins. Section 3 is devoted to the formulation of the multiperiod voltage optimization problem considering the PL flexibility. Section 4 describes the case studies based on the IEEE-123 node test feeder and presents the results. Section 5 concludes the paper.

2. EV parking lot model and flexibility optimization

The EV parking lot model described in this section focuses on representing the flexibility margins that can be offered to the DSO. It is assumed that power injection from the parking lot to the grid is not allowed. The consideration of vehicle-to-grid (V2G) exchanges deserves further research, as it requires a specific study of the pricing of the energy provided by the parking lot.

To better circumvent the limitations of booking service approaches, such as sudden or unexpected departures (i.e., departures before the booked period), the proposed model is based on scenario-based stochastic optimization. The scenarios and the corresponding probabilities are

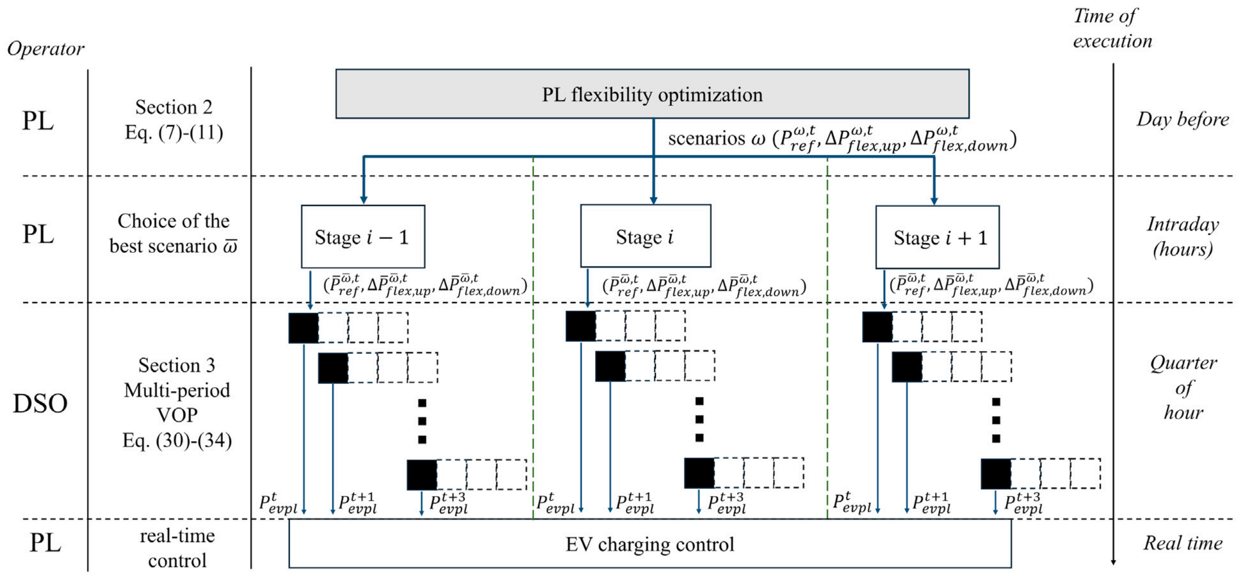

Fig. 2. The overall methodology: task organization and related time horizon for both EV PL and DSO.

obtained by forecasting the number of vehicles entering and leaving the parking lot in each period of the following day. These forecasts and the criterion to build the set of scenarios are obtained from the relevant information of the previous days or analogous days of the previous weeks and months.

The procedure has been implemented as a day-ahead evaluation considering a 4-stage stochastic approach (one day-ahead stage and three intraday stages at the end of each 6-h interval, when the day-ahead evaluation is updated to take advantage of information on the actual number of the EVs in the PL). The adopted time discretization is $\Delta t = 15$ min.

The reference value of the profile is obtained for each stage by grouping similar scenarios in a scenario tree. The scenario generation procedure assumes that forecasts of the number of EVs entering and exiting the PL in each period of the next day are available. The procedure begins by creating scenarios for the next day by multiplying the forecast profile by $1 + k_t$, where k_t is randomly generated using a normal distribution with a mean of zero and a standard deviation of $\sqrt{1-\psi_t{}^2}$, where ψ_t is a decreasing function of t to represent increasing forecast uncertainty throughout the day. Each value is rounded to the nearest positive integer, and the order of departing EVs is adjusted to ensure that the number of parked EVs never becomes negative. The initial energy of vehicles entering the PL follows a truncated normal distribution. In the tests, the corresponding mean and standard deviation are assumed to be equal to 30% of the battery size.

At each stage, the k-medoid clustering procedure from [36,37] is used to create the scenario tree. Starting with a single cluster in the day-ahead stage, each cluster can produce up to three different clusters in the next stage. For each cluster and each stage, this procedure provides the medoid (i.e., one of the original scenarios that minimizes the dissimilarity measure with respect to the other scenarios in the cluster) and the corresponding probability value π^{ω}, ensuring an integer number of entering, exiting, and parked cars, thus preserving the feasibility of the scenarios.

As a result of the scenario tree construction, sets $S^{\omega,t}_{\text{in}}$ and $S^{\omega,t}_{\text{out}}$ of entering and leaving EVs are defined, for each scenario ω and period t. The aggregated storage size $E^{\omega,t}_{\text{Smax}}$ of the PL and the maximum charging power $P^{\omega,t}_{\text{max}}$ are derived by summing the corresponding data of the individual arriving and departing vehicles.

For each time period t, scenario ω is characterized by $E^{\omega,t}_{\text{S+}}$ and $E^{\omega,t}_{\text{S-}}$, which represent the total energy stored in the EVs arriving and departing the PL, respectively. Departing vehicles are either fully charged or charged to the maximum level compatible with the charging station's rated power and parking time.

In addition, EVs entering and exiting in the same periods are grouped using two matrices: $E^{\omega,t}_{\text{ini},j}$, which sums the initial charge of EVs entering in period j and exiting in period t, and $E^{\omega,t}_{\text{g},j}$, which sums the energy gain (i.e., the difference between the final charge and the initial charge) of EVs entering in period j and leaving in period t.

Using the scenario tree, the procedure implements an optimization model (described in Section 2.1) to compute the reference profile $P^{\omega,t}_{\text{ref}}$ and performs repeated optimizations (Section 2.2) to determine maximum allowed increase $\Delta P^{\omega,t}_{\text{flex up}}$ or decrease $\Delta P^{\omega,t}_{\text{flex down}}$ in the PL power consumption for each period.

The model calculates flexibility margins assuming the DSO request is limited to a single 15-min period t_{flex}. It then repeats the calculation for additional consecutive 15-min periods n^{+}_{flex} following t_{flex}, ensuring that the flexibility margin remains constant throughout.

The agreement between the PL operator and the DSO allows the PL to recover the power change during a specified period n_{rec} after the flexibility interval. The recovery is proportional to the change in the reference profile requested by the DSO and follows a uniform pattern, with no further changes requested during n_{rec}.

$P^{\omega,t}_{\text{ref}}$, $\Delta P^{\omega,t}_{\text{flex}}$, and associated recovery profiles are provided to the DSO voltage optimization procedure as flexibility margins at the beginning of each stage for each 15 min period.

The stochastic optimal solution generates multiple potential decisions beyond the first stage. At the beginning of each intraday stage, a procedure selects the scenario $\bar{\omega}$ that minimizes the deviation from the actual number of vehicles in the PL.

As an aggregated model, the individual charging station is not treated as an independent unit in the stochastic optimization. This approach guarantees computational feasibility even in the case of a significant number of charging stations. Aggregation includes the possibility that energy can be shared among the vehicles connected to the charging stations. However, vehicle-to-vehicle (V2V) exchanges involve losses in the converters that must be accounted for. In addition, V2V exchanges may cause some stress on the battery that should be compensated or limited. Therefore, the objective function of the model includes a cost term that represents the reward that the parking lot operator should provide to the vehicle owners for the temporary use of the initial energy in the battery and the strain on the battery due to V2V exchanges. In addition, these V2V exchanges can be prohibited. This is achieved by representing the global V2V energy exchanges for each time period in the optimization model.

2.1. Reference consumption profiles

The objective function for the day-ahead calculation of the consumption profile $P^{\omega,t}$ of the PL is to minimize the procurement costs, taking into account the probability π^{ω} of each scenario ω:

$$\min \sum_{\omega} \pi^{\omega} \sum_{t} \left(\rho^{t}_{TOU} P^{\omega,t} \Delta t + C^{\omega,t}_{\mathrm{S}} \right) \tag{1}$$

where ρ^{t}_{TOU} is the time-of-use electricity tariff, $P^{\omega,t}\Delta t$ is the power consumed by the PL from the grid, and $C^{\omega,t}_{\mathrm{S}}$ is the cost associated with compensating vehicle owners for the strain on the battery due to V2V exchanges and the temporary use of the initial energy stored in the EVs at entry.

V2V exchanges are allowed by bidirectional charging stations and help to ensure that EVs depart with the maximum charge allowed by the parking duration, $E^{\omega,t}_{\mathrm{S-}}$, by using the energy stored in EVs that are expected to have longer parking times.

Scenarios in which the PL is unable to meet the charge request of some EVs, which therefore leave with lower energy levels, can be enabled by introducing a penalty into the objective function. This possibility is not addressed in the case studies of this paper. In real-time control, simple countermeasures against sudden departures are the discharge limits, which are set with respect to the initial charge and a predefined charge level reached previously (e.g., a few minutes before).

The energy balance equation for the PL is:

$$\begin{aligned} E^{\omega,t}_{\mathrm{S\ net}} &= (1-\delta)E^{\omega,(t-1)}_{\mathrm{S\ net}} + E^{\omega,t}_{\mathrm{ch,grid}} - E^{\omega,t}_{\mathrm{S-}} + \\ &\mu^{\omega,t} E^{\omega,t}_{\mathrm{S+}} - l^{\omega,t}_{\mathrm{V2V}} + \sum_{j=1}^{t} (1-\mu^{\omega,j}) E^{\omega,t}_{\mathrm{ini},\,j} \end{aligned} \tag{2}$$

$E^{\omega,t}_{\mathrm{S\ net}}$ is the total energy stored in the parked EVs in scenario ω at the end of period t. It takes into account the self-discharge rate of EV batteries δ, the energy supplied by the grid $E^{\omega,t}_{\mathrm{ch,grid}} = \eta_{\mathrm{ch}}\ P^{\omega,t}\Delta t$, and the possible use of part of the initial energy $E^{\omega,t}_{\mathrm{S+}}$ for V2V purposes (specifically $\mu^{\omega,t} E^{\omega,t}_{\mathrm{S+}}$). Variable $\mu^{\omega,t}$, which is non-negative and subject to an upper bound $\mu^{\omega,t}_{\max}$, represents the fraction of the initial energy used to ensure that a minimum energy margin $e_{\min}$ is maintained in the EV batteries.

The cost of using the initial energy of the EVs and V2V exchanges is $C^{\omega,t}_{\mathrm{S}} = \rho_{\mu} \left(\mu^{\omega,t} E^{\omega,t}_{\mathrm{S+}} + E^{\omega,t}_{\mathrm{V2V}} \right)$, where ρ_{μ} is the predefined tariff, which can be interpreted as the remuneration for the vehicles providing the service.

The energy losses $l^{\omega,t}_{\mathrm{V2V}}$ associated to V2V energy exchanges are represented by

$$l^{\omega,t}_{\mathrm{V2V}} \geq \left(1-\eta_{\mathrm{V2V}}\right) \left(E^{\omega,t}_{\mathrm{V2V}} + \mu^{\omega,t} E^{\omega,t}_{\mathrm{S+}} \right) \tag{3}$$

where η_{V2V} is the efficiency of the V2V energy exchanges, taking into account losses in power converters and batteries. Both η_{ch} and η_{V2V} are constant (i.e., the dependence of the efficiencies on the power exchanged, the state of charge, and the state of health of the batteries involved is neglected). This assumption is useful to preserve the linearity of the model and is considered reasonable due to the lack of detailed data for the public parking operator on the different types of batteries in the vehicles connected to the charging stations. Long-term efficiency degradation due to aging is not considered.

The evaluation of non-negative $E^{\omega,t}_{\mathrm{V2V}}$ is based on the observation that in the presence of V2V energy exchanges, some EVs receive more energy from the grid than needed for their final charge gain during parking. Therefore,

$$E^{\omega,t}_{\mathrm{V2V}} = E^{\omega,t}_{\mathrm{ch,grid}} - \sum_{j=1}^{t-1} E^{\omega,t}_{\mathrm{ch}\ j} \tag{4}$$

which represents the excess grid energy used for V2V exchanges. Non-negative variables $E^{\omega,t}_{\mathrm{ch}\ j}$ are the minimum load profiles necessary to ensure adequate charging for vehicles arriving in period j before they leave the parking lot. The constraints that represent $E^{\omega,t}_{\mathrm{ch}\ j}$ are

$$\begin{aligned} &\sum_{t=j+1}^{i} E^{\omega,t}_{\mathrm{ch},\,j} - \sum_{t=j+1}^{i} E^{\omega,t}_{\mathrm{g},\,j} \geq 0 \quad \text{for all } i < \tau \\ &\sum_{t=1}^{j} E^{\omega,t}_{\mathrm{ch},\,j} = 0 \qquad \sum_{t=j+1}^{\tau} E^{\omega,t}_{\mathrm{ch},\,j} - \sum_{t=j+1}^{\tau} E^{\omega,t}_{\mathrm{g},\,j} = 0 \end{aligned} \tag{5}$$

where τ is the departure period of the last EV among those entered in period j.

If the charging stations are not bidirectional, both μ and $E^{\omega,t}_{\mathrm{V2V}}$ are constrained to be zero.

Non-negative variable $E^{\omega,t}_{\mathrm{S\ net}}$ is constrained as

$$E^{\omega,t}_{\mathrm{S\ net}} \leq E^{\omega,t}_{\mathrm{Smax}} - \sum_{j=1}^{t} (1-\mu^{\omega,j}) E^{\omega,t}_{\mathrm{ini},\,j} \tag{6}$$

Moreover,

$$P^{\omega,t} \leq \min\left(P_{\mathrm{max,grid}}, P^{\omega,t}_{\mathrm{max}}\right) \tag{7}$$

where $P_{\mathrm{max,grid}}$ is the power limit of the PL connection to the external grid.

The solution of problem (1)–(7) gives the reference profile $P^{\omega,t}_{\mathrm{ref}} = P^{\omega,t}$ for all scenarios ω.

2.2. Maximum power flexibility

The maximum power reduction and increase margins are calculated for each period, considering both the single period t_{flex} and additional consecutive periods n^{+}_{flex}, up to a maximum limit of $n^{+}_{\mathrm{max,flex}}$.

The objective function is

$$\min \sum_{\omega} \pi^{\omega} \sum_{t} \left(\rho^{t}_{TOU} P^{\omega,t} \Delta t + C^{\omega,t}_{\mathrm{S}} - W^{\omega,t}_{\mathrm{flex}} \right) \tag{8}$$

where non-negative $W^{\omega,t}_{\mathrm{flex}}$ is the revenue associated with the provision of the maximum flexibility:

$$W^{\omega,t}_{\mathrm{flex}} = \begin{cases} \rho^{t}_{\mathrm{flex}}\ \Delta P^{\omega,t}_{\mathrm{flex}}\ \Delta t & \text{if } t_{\mathrm{flex}} \leq t \leq t_{\mathrm{flex}} + n^{+}_{\mathrm{flex}} \\ 0 \quad \text{otherwise} \end{cases} \tag{9}$$

Predefined tariff ρ^{t}_{flex} is the compensation rate that the DSO pays to the flexibility provider for achieving power changes $\Delta P^{\omega,t}_{\mathrm{flex\ up}}$ and $\Delta P^{\omega,t}_{\mathrm{flex\ down}}$ relative to the reference power level $P^{\omega,t}_{\mathrm{ref}}$. The up and down changes are defined as

$$\begin{aligned} \Delta P^{\omega,t}_{\mathrm{flex\ up}} &= P^{\omega,t} - P^{\omega,t}_{\mathrm{ref}} \\ \Delta P^{\omega,t}_{\mathrm{flex\ down}} &= P^{\omega,t}_{\mathrm{ref}} - P^{\omega,t} \end{aligned} \tag{10}$$

The model allows the PL to recover the power change over a predefined number of periods n_{rec} after $t_{\mathrm{flex}} + n^{+}_{\mathrm{flex}}$ (with $n_{\mathrm{rec}} = 3$ in the tests). $\Delta P^{\omega,t}_{\mathrm{flex}}$ is constrained to be uniform in the recovery interval by:

$$\begin{aligned} &\Delta P^{\omega,t}_{\mathrm{flex}} \geq -\sum_{j=t_{\mathrm{flex}}}^{t_{\mathrm{flex}}+n^{+}_{\mathrm{flex}}} \frac{\Delta P^{\omega,j}_{\mathrm{flex}}}{n_{\mathrm{rec}}} \\ &\text{for } t_{\mathrm{flex}} + n^{+}_{\mathrm{flex}} < t \leq t_{\mathrm{flex}} + n^{+}_{\mathrm{flex}} + n_{\mathrm{rec}} \\ &\Delta P^{\omega,t}_{\mathrm{flex}} = 0 \quad \text{for } t < t_{\mathrm{flex}} \text{ and } t > t_{\mathrm{flex}} + n^{+}_{\mathrm{flex}} + n_{\mathrm{rec}} \end{aligned} \tag{11}$$

The inequality in (11) becomes an equality in the flex-up scenario to prevent the use of incremental losses (such as unnecessary V2V exchanges) to enhance the flexibility margin.

In the case of multiple consecutive flexibility periods, the maximum margin is constrained to remain constant:

$$\Delta P^{\omega,t}_{\mathrm{flex}} = \Delta P^{\omega,t_{\mathrm{flex}}}_{\mathrm{flex}} \quad \text{for } t_{\mathrm{flex}} < t \leq t_{\mathrm{flex}} + n^{+}_{\mathrm{flex}}. \tag{12}$$

All models are supplemented with non-anticipativity constraints, which are common in stochastic optimization, to ensure that decisions made at various stages are based solely on currently available information, regardless of future outcomes or information.

3. Multi-period voltage optimization

During daily operation, the DSO aims at optimizing the voltage profile of the distribution grid by using the flexibility provided by PLs and other DERs. As shown in Fig. 2, the voltage optimization is a dispatching activity performed on a short time horizon, f.i. every quarter of hour, but considering also the subsequent time intervals to account for the energy recovery by PLs after flexibility has been used. This represents a significant improvement with respect to the approach presented in [34]. Due to the short time horizon, the uncertainties associated with variations of uncontrolled loads and to DERs exploiting RESs can be neglected. However, since the proposed VOP results to be highly efficient from the computational point of view, the frequency of its solution could be increased to reduce the effect of these uncertainties.

In this section, it is assumed that N_{evpl} PLs, N_{der} DERs of other types, and uncontrolled loads are connected to the distribution network. Due to the high power typically absorbed by PLs, balanced operation is assumed for the supplying MV distribution system. Concerning the PLs, for the sake of simplicity but without loss of generality, it is assumed $n^{+}_{\text{flex}} = 0$ and that n_{rec} is the same for all the PLs. Finally, barred symbol notation is adopted in which $\bar{a}$ represents a specific value assumed by the variable a.

In the following subsections, first the PL model for the VOP problem is presented and the models of the other DERs are recalled; then, the multi-period optimization problem is defined and finally expressed in variation form with respect to a reference operating point.

3.1. PL model for VOP

For the kth PL, the intraday procedure selects, at the beginning of each stage, the scenario $\bar{\omega}_k$ that best matches the actual operation of the PL in terms of number of vehicles. According to the methodology described in Section 2, the PL aggregator determines and communicates to the DSO the values of the three non-negative variables $\bar{P}^{\bar{\omega}_k,t}_{\text{ref},k}$, $\bar{\Delta P}^{\bar{\omega}_k,t}_{\text{flex down},k}$ and $\bar{\Delta P}^{\bar{\omega}_k,t}_{\text{flex up},k}$.

At time period t, the active power absorbed by the N_{evpl} PLs is modeled by

$$P^{t}_{\text{evpl},k} = \bar{P}^{\bar{\omega}_k,t}_{\text{ref},k} + P^{t}_{\text{flex up},k} - P^{t}_{\text{flex down},k} + \bar{R}^{n_{\text{rec}},t}_{\text{down},k} - \bar{R}^{n_{\text{rec}},t}_{\text{up},k} \qquad \text{for } k = 1,\dots,N_{\text{evpl}} \tag{13}$$

where $P^{t}_{\text{flex up},k}$ and $P^{t}_{\text{flex down},k}$ are the upward and downward flexibility to be used, respectively, and $\bar{R}^{n_{\text{rec}},t}_{\text{up},k}$ and $\bar{R}^{n_{\text{rec}},t}_{\text{down},k}$ are the active power to be recovered for the upstream and downstream flexibilities used in the previous n_{rec} periods, respectively. They are given by

$$\bar{R}^{n_{rec},t}_{\text{up},k} = \frac{1}{n_{\text{rec}}}\sum_{i=1}^{n_{\text{rec}}} \bar{P}^{t-i}_{\text{flex up},k}\,,\quad \bar{R}^{n_{\text{rec}},t}_{\text{down},k} = \frac{1}{n_{\text{rec}}}\sum_{i=1}^{n_{\text{rec}}} \bar{P}^{t-i}_{\text{flex down},k} \tag{14}$$

being $\bar{P}^{t-i}_{\text{flex up},k}$ and $\bar{P}^{t-i}_{\text{flex down},k}$ the values of, respectively, the upward and downward flexibility obtained by the VOP solution in the previous time period $t-i$ for the kth PL.

In addition to (13), the following inequalities must be satisfied for non-negative $P^{t}_{\text{flex up},k}$ and $P^{t}_{\text{flex down},k}$

$$P^{t}_{\text{flex up},k} \le \begin{cases} 0 & \text{if } \bar{R}^{n_{\text{rec}},t}_{\text{up},k} > 0 \\ \max\left(0, \bar{\Delta P}^{\bar{\omega}_k,t}_{\text{flex up},k} - \bar{R}^{n_{\text{rec}},t}_{\text{down},k}\right) & \text{otherwise} \end{cases} \tag{15}$$

$$P^{t}_{\text{flex down}} \le \begin{cases} 0 & \text{if } \bar{R}^{n_{\text{rec}},t}_{\text{down},k} > 0 \\ \max\left(0, \bar{\Delta P}^{\bar{\omega}_k,t}_{\text{flex down},k} - \bar{R}^{n_{\text{rec}},t}_{\text{up},k}\right) & \text{otherwise} \end{cases} \tag{16}$$

$$P^{t}_{\text{flex up},k}\, P^{t}_{\text{flex down},k} \le 0 \tag{17}$$

$$\text{for } k = 1,\dots,N_{\text{evpl}}$$

Constraint (15) allows variable $P^{t}_{\text{flex up},k}$ to be non-zero only if, in the previous n_{rec} time periods, upward flexibility has not been used, and if recovering the used downward flexibility does not consumes all the upward flexibility permitted by the value $\bar{\Delta P}^{\bar{\omega}_k,t}_{\text{flex down},k}$ set by the PL aggregator. Constraint (16) imposes a similar condition on the variable $P^{t}_{\text{flex down},k}$. Constraint (17) prevents both $P^{t}_{\text{flex up},k}$ and $P^{t}_{\text{flex down},k}$ from being non-zero at the same time.

Finally, n_{rec} equality constraints must be added regarding the recovered energy. The need to recover the flexibility once it has been used introduces another relationship between the VOPs solved at time t and those to be solved in the following n_{rec} time periods. Then, a multi-period approach must be adopted, in which the VOP at time t accounts for the impact of the non-zero values of $P^{t}_{\text{flex up},k}$ or $P^{t}_{\text{flex down},k}$ on subsequent time periods through the values of $\bar{R}^{n_{\text{rec}},t+j}_{\text{up},k}$ and $\bar{R}^{n_{\text{rec}},t+j}_{\text{down},k}$. Using (13)–(14) the following additional n_{rec} equality constraints are derived:

$$\begin{aligned} P^{t+j}_{\text{ev pl},k} = {} & \bar{P}^{\bar{\omega}_k,t+j}_{\text{ref},k} + \frac{1}{n_{\text{rec}}}\left(P^{t}_{\text{flex down},k} - P^{t}_{\text{flex up},k}\right) \\ & + \bar{R}^{n_{\text{rec}},t+j}_{\text{down},k} - \bar{R}^{n_{\text{rec}},t+j}_{\text{up},k} \\ & \text{for } j = 1,\dots,n_{\text{rec}} \quad \text{for } k = 1,\dots,N_{\text{evpl}} \end{aligned} \tag{18}$$

where

$$\begin{aligned} \bar{R}^{n_{\text{rec}},t+j}_{\text{up},k} &= \frac{1}{n_{\text{rec}}}\sum_{i=1+j}^{n_{\text{rec}}} \bar{P}^{t+j-i}_{\text{flex up},k} \\ \bar{R}^{n_{\text{rec}},t+j}_{\text{down},k} &= \frac{1}{n_{\text{rec}}}\sum_{i=1+j}^{n_{\text{rec}}} \bar{P}^{t+j-i}_{\text{flex down},k} \end{aligned} \tag{19}$$

3.2. Other DER models for VOP

At time period t, the operational ranges of the N_{der} DERs are modeled as variations in both active and reactive powers ($P^{t}_{\text{der},h}$ and $Q^{t}_{\text{der},h}$) within specified minimum values ($\bar{P}^{t}_{\text{der min},h}$ and $\bar{Q}^{t}_{\text{der min},h}$) and maximum values ($\bar{P}^{t}_{\text{der max},h}$ and $\bar{Q}^{t}_{\text{der max},h}$); that is:

$$\begin{aligned} &\bar{P}^{t}_{\text{der min},h} \le P^{t}_{\text{der},h} \le \bar{P}^{t}_{\text{der max},h} \\ &\qquad\qquad \text{for } h = 1,\dots,N_{\text{der}} \\ &\bar{Q}^{t}_{\text{der min},h} \le Q^{t}_{\text{der},h} \le \bar{Q}^{t}_{\text{der max},h} \end{aligned} \tag{20}$$

3.3. Multi-period objective function

In this paper, the objective of the DSO operation is to optimize the voltage profiles along all feeders. Other objectives, such as network loss minimization, can be addressed in a similar way.

Monitoring all node voltages in a large distribution system is not feasible; to address this issue, the distribution network is partitioned into N_{vcz} virtual voltage control zones (VCZs). In each VCZ, a pilot node (PN) is identified, whose voltage adequately represents the voltage amplitudes of all nodes in that VCZ, as described in [38]. The objective of the VOP is defined as

$$\min_{\boldsymbol{x}^t} \sum_{i=1}^{N_{\text{vcz}}}\sum_{j=0}^{n_{\text{rec}}} \left(\left(V^{t+j}_{\text{pn},i}\right)^2 - \bar{V}^2_{\text{pn ref},i}\right)^2 \tag{21}$$

where $V^{t+j}_{\text{pn},i}$ and $\bar{V}_{\text{pn ref},i}$ are the voltage amplitude and the assigned reference value for the PN of the ith VCZ at time $t+j$, respectively. The objective function in (21) is the sum of the squared voltage deviations of the PNs in the current time period t and in the subsequent n_{rec} time periods. This formulation accounts for the impact of the variables $P^{t}_{\text{flex up},k}$ and $P^{t}_{\text{flex down},k}$ on the subsequent time periods through (18).

Defining

$$y_{\text{pn}}^{t+j} = \left[\left(V_{\text{pn},1}^{t+j}\right)^2, \ldots, \left(V_{\text{pn},N_{vcz}}^{t+j}\right)^2\right]^T \tag{22}$$

and a similar expression for the vector of reference values, the objective function (21) is rewritten in vector form

$$\min_{x^t} \sum_{j=0}^{n_{\text{rec}}} \left(y_{\text{pn}}^{t+j} - \bar{y}_{\text{pn ref}}\right)^T \left(y_{\text{pn}}^{t+j} - \bar{y}_{\text{pn ref}}\right) \tag{23}$$

The vector of optimization variables x^t for the time period t under consideration includes the active and reactive powers of the DERs, as well as the up and down flexibility of the PLs according to

$$x^t = \left[x_{der}^{t\ T}\ \ x_{\text{flex up}}^{t\ \ T}\ \ x_{\text{flex down}}^{t\ \ T}\right]^T \tag{24}$$

in which

$$x_{\text{der}}^{t\ T} = \left[P_{\text{der},1}^t, \ldots, P_{\text{der},N_{der}}^t, Q_{\text{der},1}^t, \ldots, Q_{\text{der},N_{der}}^t\right]^T$$

$$x_{\text{flex up}}^{t\ \ T} = \left[P_{\text{flex up},1}^t, \ldots, P_{\text{flex up},N_{\text{evpl}}}^t\right]^T$$

$$x_{\text{flex down}}^{t\ \ T} = \left[P_{\text{flex down},1}^t, \ldots, P_{\text{flex down},N_{\text{evpl}}}^t\right]^T$$

3.4. System constraints

The VOP should also include the system constraints, particularly the power flow equations that relate the voltage amplitudes $V_{\text{pn},i}^{t+j}$ of the PNs in (23) to the optimization variables x^t. In large distribution networks, the power flow equations represent a significant number of non linear equations. In addition, since multiple time periods are considered in (21), the power flow equations need to be repeated $n_{rec}+1$ times. This repetition leads to a considerable increase in computational burden and a risk of convergence problems in the VOP numerical solution. To avoid such drawbacks, the constrained Jacobian method proposed in [32] is used, which takes advantage of the radial configuration of the network. According to this method, the power flow equations are replaced by their linearization around a given operating point, which is obtained by a single base-case power flow calculation. The model was implemented with reference to the balanced systems and operating conditions. The square amplitudes of the nodal voltages (22) are linearly related to the variations of the active and reactive powers injected in each node with respect to their values in the base case, represented by superscript 0, as follows

$$\begin{aligned} y_{\text{pn}}^{t+j} &= \bar{y}_{\text{pn}}^0 + \Gamma_{\text{der}}\left(x_{\text{der}}^{t+j} - \bar{x}_{\text{der}}^0\right) - \Gamma_{\text{evpl}}\left(x_{\text{evpl}}^{t+j} - \bar{x}_{\text{evpl}}^0\right) \\ &\quad - \Gamma_{\text{load}}\left(\bar{x}_{\text{load}}^{t+j} - \bar{x}_{\text{load}}^0\right) \qquad j = 0, \ldots, n_{\text{rec}} \end{aligned} \tag{25}$$

where

$$x_{\text{evpl}}^{t+j} = \left[P_{\text{evpl},1}^{t+j}, \ldots, P_{\text{evpl},N_{\text{evpl}}}^{t+j}\right]^T$$

and the vector $\bar{x}_{\text{load}}^{t+j}$ includes the active and reactive powers absorbed by uncontrolled loads. In (25) the matrices Γ_{der}, Γ_{evpl} and Γ_{load} are fixed sensitivity matrices which are off-line evaluated in some typical operating conditions of the distribution system, f.i. high/medium/low loading conditions according to [32]. On the contrary, for the VOP formulation, the base-case values refer to the real-time actual operating conditions of distribution system.

Rewriting the PL model Eqs. (13) and (18) in vector form yields, respectively,

$$x_{\text{evpl}}^t = x_{\text{flex up}}^t - x_{\text{flex down}}^t + \bar{x}_{\text{ref rec}}^t \tag{26}$$

$$x_{\text{evpl}}^{t+j} = \frac{1}{n_{rec}}\left(x_{\text{flex down}}^t - x_{\text{flex up}}^t\right) + \bar{x}_{\text{ref rec}}^{t+j} \tag{27}$$

in which the terms $\bar{x}_{\text{ref rec}}^t$ and $\bar{x}_{\text{ref rec}}^{t+j}$ include the assigned values of the reference profile ($\bar{P}_{\text{ref},k}^{\bar{\omega}_k,t}$ and $\bar{P}_{\text{ref},k}^{\bar{\omega}_k,t+j}$) and of the power recovery for the flexibility used in the previous periods ($\bar{R}_{\text{down},k}^{n_{\text{rec}},t}$, $\bar{R}_{\text{up},k}^{n_{\text{rec}},t}$, $\bar{R}_{\text{down},k}^{n_{\text{rec}},t+j}$ and $\bar{R}_{\text{up},k}^{n_{\text{rec}},t+j}$).

Substituting (26) and (27) into (25) yields

$$y_{\text{pn}}^{t+j} = \tilde{y}_{\text{pn}}^{t+j} + \Gamma_j\, x^t \quad \text{for } j = 0, \ldots, n_{\text{rec}} \tag{28}$$

being the $N_{vcz} \times 2(N_{\text{der}}+N_{\text{evpl}})$ matrices Γ_j defined as

$$\Gamma_j = \left[\Gamma_{\text{der}}, -\Gamma_{\text{evpl}}, \Gamma_{\text{evpl}}\right] \text{ for } j = 0$$

$$\Gamma_j = \frac{1}{n_{rec}}\left[\mathbf{0}, \Gamma_{\text{evpl}}, -\Gamma_{\text{evpl}}\right] \text{ for } j \neq 0$$

and $\tilde{y}_{\text{pn}}^{t+j}$ the vector that includes all the assigned terms (i.e., all the barred quantities).

Admissible range of PN voltage amplitudes have to be added to guarantee the power quality of the grid operation:

$$\bar{y}_{\text{pn min}} \le y_{\text{pn}}^{t+j} \le \bar{y}_{\text{pn max}} \qquad \text{for } j = 0, \ldots, n_{\text{rec}} \tag{29}$$

Finally, an additional inequality constraint is introduced to ensure that the costs associated with the use of DER powers and PL flexibility are less than the assigned budget b_{DSO}^t

$$c_{der}\left(x_{\text{der}}^t\right) + c_{pl}\left(x_{\text{flex up}}^t, x_{\text{flex down}}^t\right) \le b_{DSO}^t \tag{30}$$

in which c_{der} and c_{pl} are typically linear cost functions.

3.5. VOP formulation

The VOP can finally be formulated using all the equations of the previous subsections as

$$\min_{x^t} \sum_{j=0}^{n_{rec}} \left(\Gamma_j\, x^t + \tilde{y}_{\text{pn}}^{t+j} - \bar{y}_{\text{pn ref}}\right)^T \left(\Gamma_j\, x^t + \tilde{y}_{\text{pn}}^{t+j} - \bar{y}_{\text{pn ref}}\right) \tag{31}$$

subject to

$$\bar{y}_{\text{pn min}} - \tilde{y}_{\text{pn}}^{t+j} \le \Gamma_j\, x^t \le \bar{y}_{\text{pn max}} - \tilde{y}_{\text{pn}}^{t+j} \text{ for } j = 0, \ldots, n_{rec} \tag{32}$$

$$\bar{x}_{\text{min}}^t \le x^t \le \bar{x}_{\text{max}}^t \tag{33}$$

$$x_{\text{flex up}}^t \odot x_{\text{flex down}}^t \le 0 \tag{34}$$

$$c_{tot}(x^t) \le b_{DSO}^t \tag{35}$$

The objective function in (31) is quadratic and is obtained by substituting (28) into (23). The linear inequality constraints (32) are derived by substituting (28) in (29). The box constraint (33) is the vector form of inequalities (15), (16) and (20). Constraint (34) is the vector form of inequalities (17), in which the operator ⊙ represents the Schur product. Finally, constraint (35) is the compact form of inequality (30), which is typically linear.

The VOP (31)–(35) is a quadratic programming (QP) problem with linear constraints, except for (34), which ensures that at least one the two variables $P_{\text{flex up},k}^t$ and $P_{\text{flex down},k}^t$ is null. Then, to solve the VOP, a classical sequential QP algorithm can be used, solving a series of QP problems obtained by assuming only one of the two variables, that is either $P_{\text{flex up},k}^t$ or $P_{\text{flex down},k}^t$.

4. Case study

The methodology for calculating the flexibility margins was applied to 3 PLs with different characteristics. The VOP procedure was applied to a test distribution system based on the IEEE 123-nodes test feeder, with additional 15 PV units and 4 EV PLs, over a 24 h horizon. As the implemented model assumes balanced operating conditions, the IEEE 123-node test feeder data were balanced by averaging the per-phase parameters of the lines and loads.

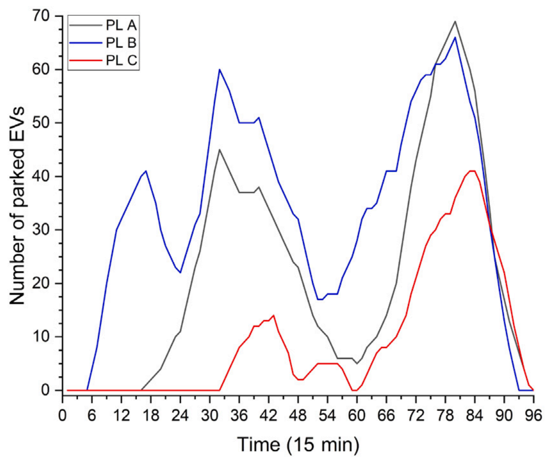

Fig. 3. Day-ahead forecasted number of EVs parked in the three PLs: PL A in black, PL B in blue, PL C in red.

Table 2
Characteristics of the EVs.

Type of EV	Size of the battery	Penetration
1	25 kWh	15%
2	45 kWh	45%
3	70 kWh	25%
4	100 kWh	15%

4.1. Parking lots

The three PLs considered in the tests are denoted as PL A, PL B, and PL C, each with a maximum power consumption of 3 MW. PL A and PL B each have 70 charging stations, while PL C has 45. In all scenarios, the PLs are empty at the beginning of the day, and all EVs leave before the day ends. The number of EVs parked in each of the three PLs at the beginning of the 96 time intervals throughout the day is forecasted and shown in Fig. 3.

These forecasts are used to generate a total of 60 different daily scenarios. The ψ_t function is assumed to decrease linearly from 0.9999 in the first period to 0.99 in the last period. Similar scenarios are grouped together using the *k*-medoid method, resulting in a 4-stage tree with nodes representing the obtained medoids. The profiles of scenarios sharing common nodes in the tree are bounded at each stage according to the tree structure.

In the tests, the types of cars are classified into 4 categories, as shown in Table 2, based on data available from various Internet sources. Although these categories seem appropriate for the current situation in certain countries, it is essential to adapt them to specific local conditions. A maximum charging power of 40 kW is assumed for each charging station, representing typical ac charging stations installed in PLs where EVs remain connected for extended periods.

For the EV batteries, δ is assumed to be zero. The charging and V2V energy transfer efficiencies, η_{ch} and η_{V2V}, are set to 0.96 and 0.92, respectively.

Time of use price ρ^t_{TOU} is set at 72.39 €/MWh from 7 am to 11 pm and to 51.62 €/MWh during other times. If $\mu^{\omega,t}_{\text{max}}$ is greater than 0, the price for using the initial EV energy is $\rho_\mu = 50$ €/MWh, which is lower than the grid price. In each period, minimum initial energy e_{min} is set to 20% of the sum of the rated capacity of the batteries of the entering EVs.

For the calculation of both the downward and upward power flexibility provided by the PL, predefined tariff ρ^t_{flex} is set at 100 €/MWh, significantly higher than the grid prices. In all cases, the recovery interval is set to $n_{\text{rec}} = 3$ periods for all the PLs.

Table 3
Maximum and average flexibility in MW.

EVPL	Flexibility	$n^+_{flex} = 0$		$n^+_{flex} = 1$		$n^+_{flex} = 2$	
		max	avg	max	avg	max	avg
PL A	Down	2.8	0.7	1.0	0.4	0.5	0.3
	Up	2.2	0.6	1.3	0.3	0.8	0.3
PL B	Down	1.7	1.0	1.4	0.6	0.5	0.2
	Up	1.4	1.0	0.7	0.4	0.5	0.4
PL C	Down	1.3	0.6	0.8	0.3	0.2	0.1
	Up	1.3	0.7	0.7	0.4	0.7	0.4

Table 4
Maximum and average values of the percentage reduction of the objective function with respect to the reference values.

EVPL	Flex	$n^+_{flex} = 0$		$n^+_{flex} = 1$		$n^+_{flex} = 2$	
		max	avg	max	avg	max	avg
PL A	Down	7.7	1.5	8.3	1.4	4.7	1.1
	Up	6.3	1.0	8.6	1.4	8.6	1.6
PL B	Down	7.5	1.3	12.1	1.4	2.2	0.6
	Up	3.5	0.9	3.5	1.0	3.6	0.9
PL C	Down	10.1	1.4	10.0	1.5	6.5	1.2
	Up	10.2	0.9	17.1	1.6	18.7	2.0

To illustrate the results of the calculation of the flexibility limits, Fig. 4 shows for the fist period of flexibility, limited to those exceeding 100 kW, for representative scenarios relevant to PL A, PL B, and PL C. The results of Fig. 4 refer to the scenarios that are assumed to correspond more closely to the actual number of parked EVs. These scenarios are used by the VOP to obtain the results shown in Section 4.2. The scenario for PL A includes 195 EVs with an average stay time of 10 periods, the scenario of PL B includes 327 EVs with an average stay time of 9.4 periods, and the scenario for PL C includes 121 EVs with average stay time of 7.4 periods. The figure shows the results obtained for a single 15-min flexibility interval ($n^+_{\text{flex}} = 0$), two consecutive intervals ($n^+_{\text{flex}} = 1$), and three consecutive intervals ($n^+_{\text{flex}} = 2$). The flexibility value remains the same in each consecutive period, and for all cases, the flexibility is recovered in the following $n_{\text{rec}} = 3$ periods, as mentioned in Section 2.2. In period 46, PL A can provide both upward and downward flexibility for $n^+_{\text{flex}} = 0$. In several cases where single-period flexibility cannot be provided, two- or three-period flexibility is allowed due to the more favorable recovery interval. PL C shows less flexibility because of the lower number of both EVs and average stay time compared to the other two PLs.

Considering all the scenarios, Table 3 shows the maximum and average values of both downward and upward flexibility for the same scenarios as those in Fig. 4. The PL C results are the lowest confirming the low flexibility. The results of PL A and PL B are closer, with PL A showing improved flexibility, due to the greater importance of stay time duration with respect to the number of EVs.

The values of the objective function (21) for the stochastic optimization case without flexibility are € 438 for PL A, € 568 for PL B, € 242 for PL C. Table 4 shows the maximum and average percentage reductions (for the different periods) with respect to the above mentioned objective function values of the case without flexibility. For all the considered PLs, the percentage reductions in the objective function (when all the flexibility is used) are significant.

The PL model have been implemented as stochastic linear programming problem in AIMMS and solved by using Gurobi.

4.2. Multi-period VOP

With respect to the network characteristics described in [39], 4 PLs and 15 PV systems have been added and connected to the IEEE 123-nodes test feeder as shown in Fig. 5. Applying the methodology

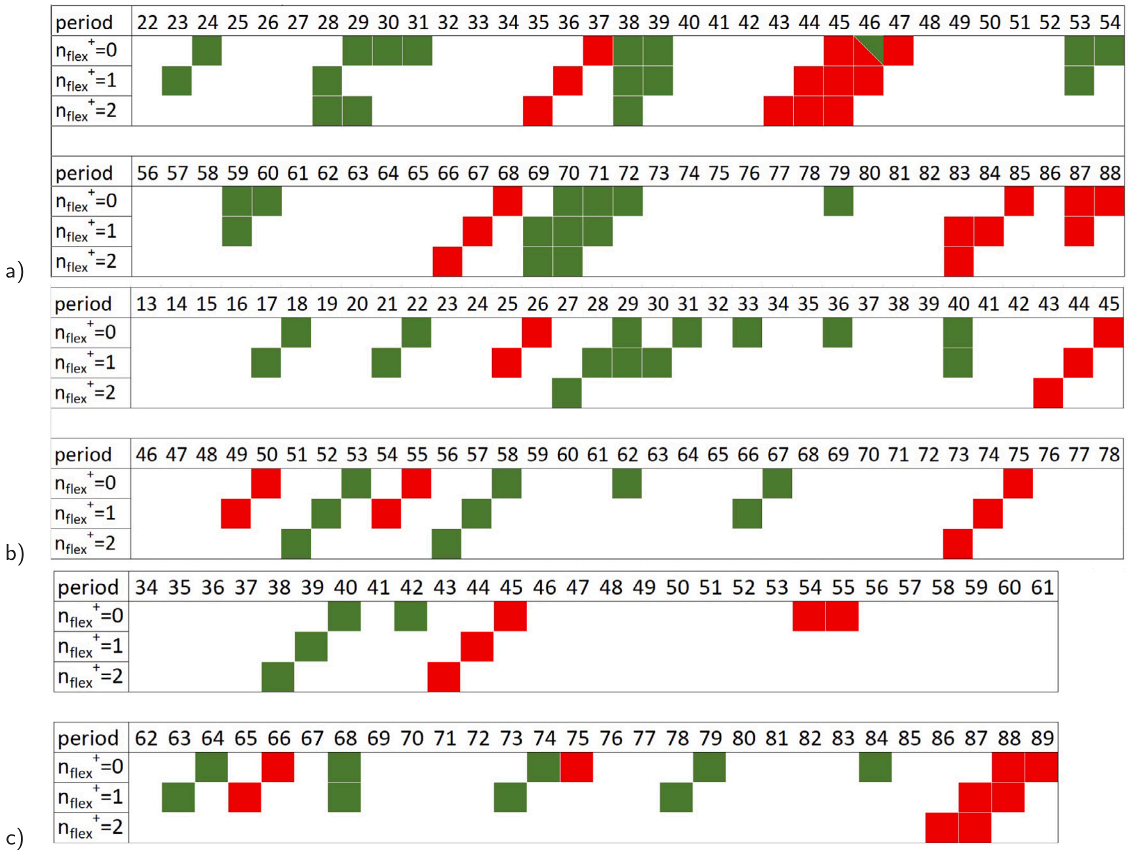

Fig. 4. Initial period of the flexibility intervals with a margin larger than 100 kW for a scenario of: (a) PL A, (b) PL B, and (c) PL C. Downward flexibility is shown in green and upward flexibility in red. The columns represent 15-min periods, and the rows indicate the maximum duration of flexibility intervals before recovery. (For interpretation of the references to color in this figure legend, the reader is referred to the web version of this article.)

Table 5
EV PL parameters given as input to the multi-period VOP.

# of PL	Type	Connection node	# of VCZ
$EVPL_1$	C	4	VCZ_1
$EVPL_2$	A	53	VCZ_2
$EVPL_3$	B	114	VCZ_3
$EVPL_4$	C	29	VCZ_4

presented in [40], the feeder has been partitioned in 4 virtual VCZs and the related 4 PNs have been identified, see Fig. 5. Table 5 lists the number of each EV PL and the type according to the PL scenarios used in Fig. 4, the connection nodes to the electricity distribution network and the VCZ to which they belong.

The PV systems all have the same rated power; two cases are considered, referred to as Case A and Case B, according to the rated power of each PV system, which is assumed equal to 200 or 300 kW, respectively. The generated active powers track the maximum power point according to the variations of the solar radiation during the day and cannot be curtailed. The resulting daily curve of the total active power generation is shown in Fig. 6 for Case A. In Case B, the same solar radiation variation is considered, resulting in a daily curve of total active power generation that is 50% larger than the one in Fig. 6. The reactive power provided by the PV system can be varied only when the generated active power is larger than 10% of the rated value; the reactive power variation is limited to keep the power factor, both leading and lagging, within 0.9 and 1.

Case A and Case B also differ in terms of system loading conditions. In case A, the load rated powers from [39] are used and the total active power load curve is shown in Fig. 6. In case B, the total daily load curve was reduced to 30% of that in Case A. Overall, Case B represents

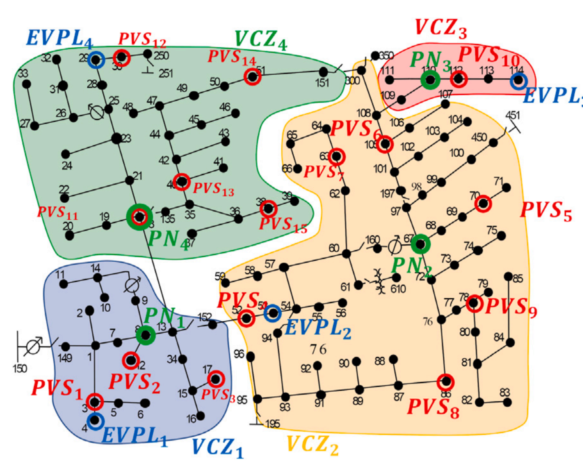

Fig. 5. Adapted IEEE 123 node test feeder.

an operating condition with lower load and higher PV generation than Case A. Regarding the PLs, identical operating conditions are assumed in both Case A and Case B.

The results are presented and compared with reference to three different VOP options:

- *no VOP*: no VOP is performed;
- *VOP DERs*: VOP is performed every 15 min by varying only DER reactive power outputs;
- *VOP DERs and PLs*: VOP is performed every 15 min by varying both DER reactive power outputs and PL absorbed powers.

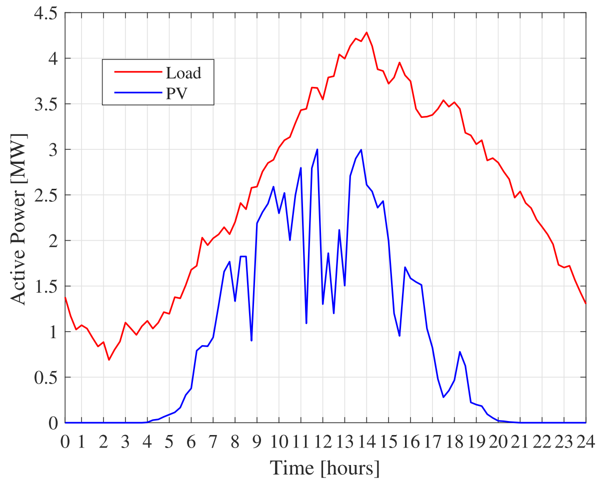

Fig. 6. Production by the 15 PVs and load consumption for Case A, characterized by 200 kW nominal production by each PV system and rated consumption by loads.

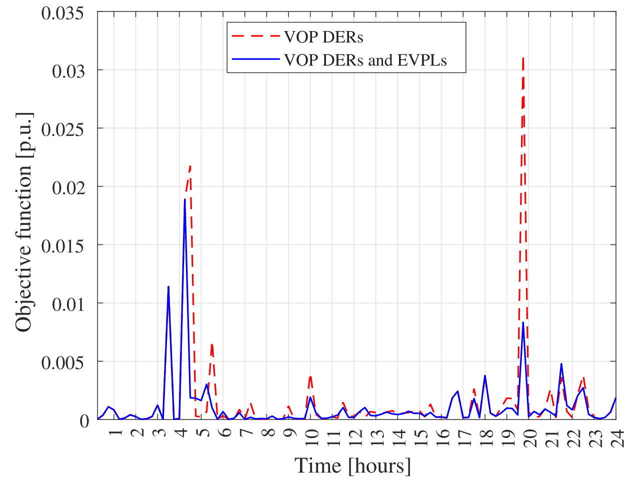

Fig. 7. Time evolution of the objective function in Case A.

Table 6
VDI for the three VOP options.

Case	*no VOP*	*VOP DERs*	*VOP DERs and PLs*
A	0.335	0.154	0.101
B	0.359	0.141	0.091

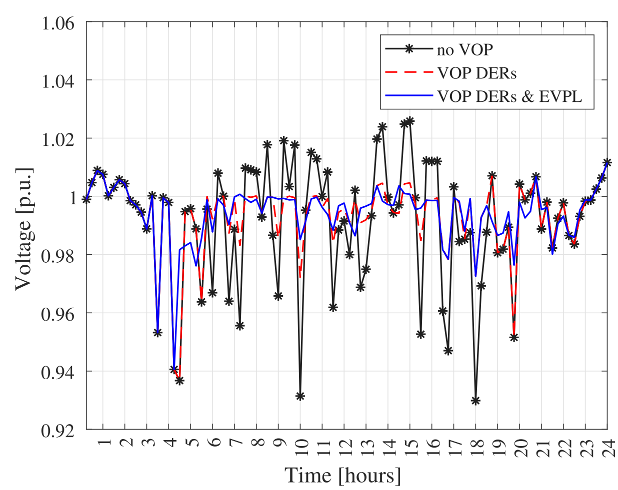

Fig. 8. PN_3 voltage profiles during the 24 h in Case A.

The results of the three algorithms are compared in terms of:

- voltage deviation index (VDI), calculated as the 24-h sum of the objective function values (21), through PF calculations every 15 min;
- actual power absorbed by the PLs during the day with respect to the scheduled power;
- total energy absorbed by the PLs over the 24 h.

Moreover, the sensitivity of the results with respect to the value assigned to the budget b^t_{DSO} in constraint (35) is also analyzed.

The VOP model was implemented and solved using a MATLAB R2022a script with the function fmincon, which allows the implementation of linear and quadratic constraints of the type shown in (34). The initial power flow calculation was performed using MatPower [41]. For the case study and the operating conditions considered, the computational effort was low. For each execution, the VOP algorithm takes on average 0.25 s with an AMD Ryzen 7 4800H, 2.9 GHz CPU and 16 GB of RAM.

4.2.1. Case A

Fig. 7 shows the time evolution of the objective function for the VOP that uses only DERs (red dashed line) and the VOP that uses both DERs and PL flexibility (blue solid line). The case of *no VOP* is not shown for readability reasons because the objective function has significantly larger values. During periods when no flexibility is allowed by the PL operators, the two lines are superimposed, and only the blue solid line is visible. During periods when PL flexibility is available, it is used by the *VOP DERs and PLs* algorithm to minimize the value of the objective function. The performance improvement was quantified using the values of VDI reported in Table 6. The introduction of VOP, which uses only the reactive power compensation capability of PV systems, allows a reduction in the VDI value by approximately 55% with respect to the *no VOP* solution, and a further reduction of approximately 34% is obtained by exploiting the PL flexibility with respect to the *VOP DERs* algorithm. As an example, the time evolution of the voltage at PN_3 in Case A for the three algorithms is shown in Fig. 8. PN_3 is chosen as it is the pilot node farthest from the supplying substation; therefore, its voltage is the most sensitive to changes in system operating conditions. The plot illustrates the mitigation of voltage variation achieved through the implementation of the VOP algorithm, especially when PL flexibility is used.

To analyze the performance of the proposed multi-period VOP in detail, Figs. 9–12 show the time evolution of active powers absorbed by $EVPL_1$–$EVPL_4$, respectively. In particular, the planned absorption is compared with the actual value obtained by the *VOP DERs and PLs* algorithm. Fig. 13 shows the recovery of the $EVPL_2$ absorption between 11:00 and 12:45: after each period in which the proposed algorithm changes the actual power from the reference value, in the following three periods ($n_{rec} = 3$) the energy variation is recovered through opposite-sign adjustments relative to the scheduled absorption. In the period between 11:30 and 11:45, the multi-period VOP uses the power flexibility offered by the $EVPL_2$ (the actual absorption, indicated by the blue curve, exceeds the scheduled one by approximately 0.27 MW); in the following three periods (between 11:45 and 12:30), the actual absorption falls below the scheduled level by approximately 0.09 MW.

Regarding the choice of flexibility, the multi-period VOP decides within a given interval whether to use the available flexibility, while also considering flexibility availability in the three subsequent intervals. This decision is based on assessing the flexibility across four periods of 15 min and selecting the interval that results in the best voltage profile. In the example shown in Fig. 13, $EVPL_2$ is of PL A type with $n^+_{\text{flex}} = 0$. As shown in Fig. 4, upward flexibility is available

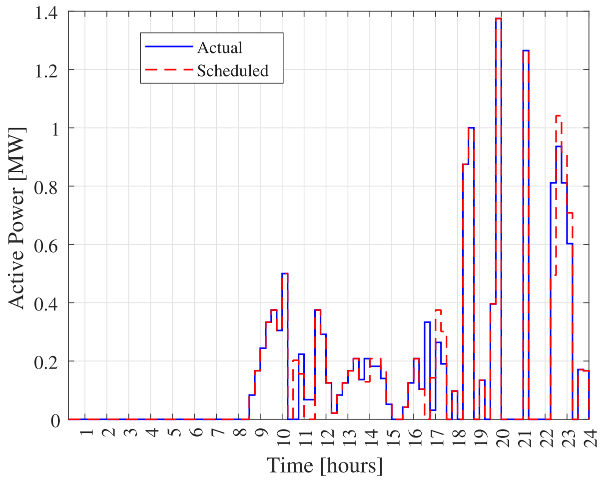

Fig. 9. PL_1 scheduled (reference) vs. optimized consumption profiles in Case A.

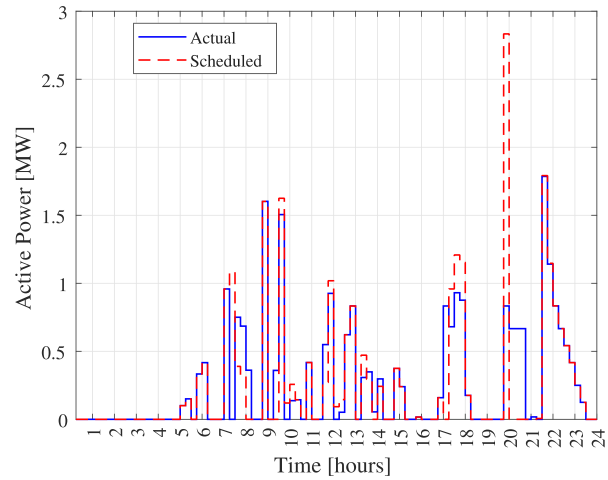

Fig. 10. PL_2 scheduled (reference) vs. optimized consumption profiles in Case A.

Table 7
Total daily energy consumed, valid for both Case A and Case B (MWh).

	$EVPL_1$	$EVPL_2$	$EVPL_3$	$EVPL_4$
Scheduled	3.6501	6.2028	8.5602	3.6501
VOP DERs and PLs	3.6501	6.2028	8.5602	3.6501

during the three intervals between 11:15 and 12:00 (periods 45, 46, and 47 in Fig. 4). The multi-period VOP chooses to use the flexibility in period 46 as it ensures a better voltage profile compared to using it in intervals 45 or 47. The multi-period VOP is aware that once upward flexibility is used in interval 46, it cannot be used again in the following three intervals, due to the downward recovery requirement.

As a final observation, although the multiperiod VOP cannot apply the same upward flexibility during the recovery intervals, if downward flexibility is available during the recovery periods, it can be used in addition to the ongoing downward recovery. An example is shown in Fig. 14 for $EVPL_3$ (PL B type) between 13:45 and 14:45. The actual absorbed power (blue line) between 14:30 and 14:45 (the third recovery period) is much lower than the scheduled profile compared to the reductions in the previous two intervals. Indeed, in this third recovery period (period 58 in Fig. 4), the $EVPL_3$ has downward flexibility available, which is added to the downward recovery. The additional downward flexibility is recovered over the three subsequent intervals between 14:45 and 15:30.

The effectiveness of the energy recovery imposed by the proposed algorithm was verified using the results obtained in terms of the total energy absorbed by the PLs throughout the day. Table 7 shows that the energy values for the scheduled program, that is, the energy absorbed by each PL without any flexibility, and for the multi-period VOP, that is, the actual energy absorbed according to the results of the proposed algorithm, are the same. This ensures the adequacy of the EV charging service.

4.2.2. Case B

Fig. 15 compares the time evolution of the objective function for the VOP with only DERs (red dashed line) and the VOP with both DERs and PLs flexibility (blue solid line). In addition, the results show that the *VOP DERs and PLs* algorithm uses PL flexibility to minimize the objective function value whenever it is available. The performance improvement was quantified using the VDI values reported in Table 6. In Case B, the VOP that uses only the reactive power compensation by the PV systems allows a reduction of the VDI value by about 61% compared to the *no VOP* algorithm, with a further reduction of about 35% is obtained by also exploiting the flexibility of PLs with respect to the *VOP DERs* algorithm.

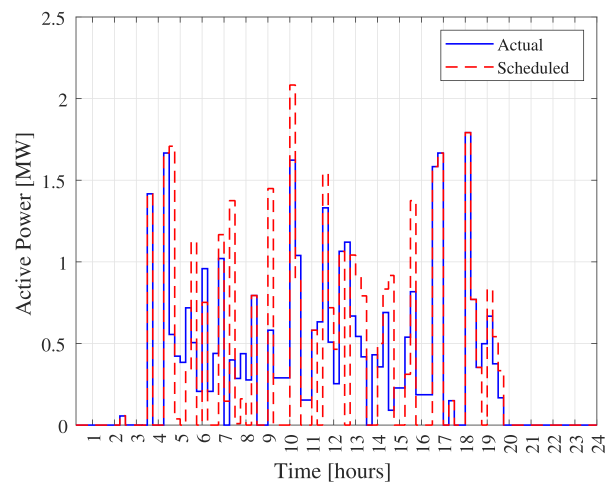

Fig. 11. PL_3 scheduled (reference) vs. optimized consumption profiles in Case A.

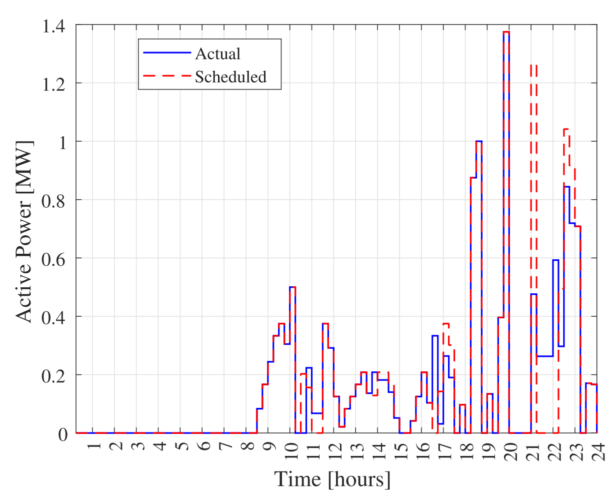

Fig. 12. PL_4 scheduled (reference) vs. optimized consumption profiles in Case A.

The time evolution of voltage at PN_3 is shown as an example in Fig. 16. The plot demonstrates the voltage variation control achieved by implementing the VOP algorithm, especially when the flexibility of the PLs is exploited.

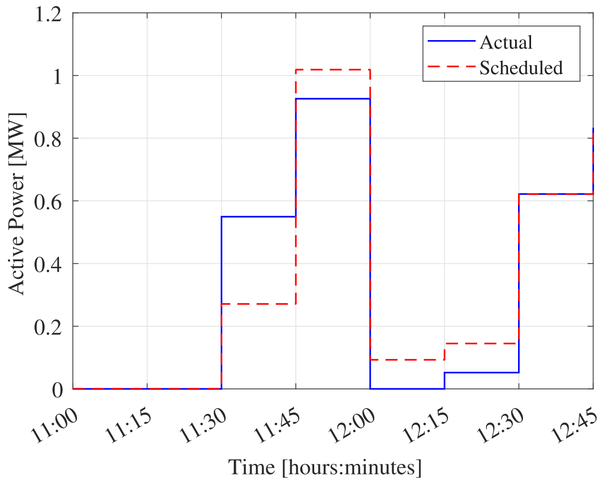

Fig. 13. PL_2 scheduled (reference) vs. optimized consumption profiles in Case A, between 11:00, and 12:45.

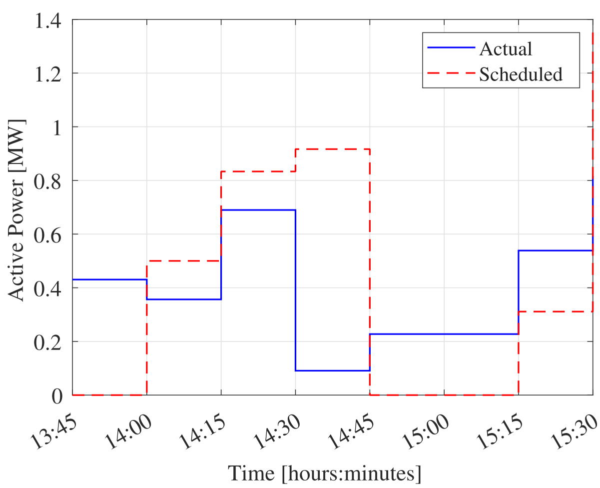

Fig. 14. PL_3 scheduled (reference) vs. optimized consumption in Case A, between 13:45, and 15:30.

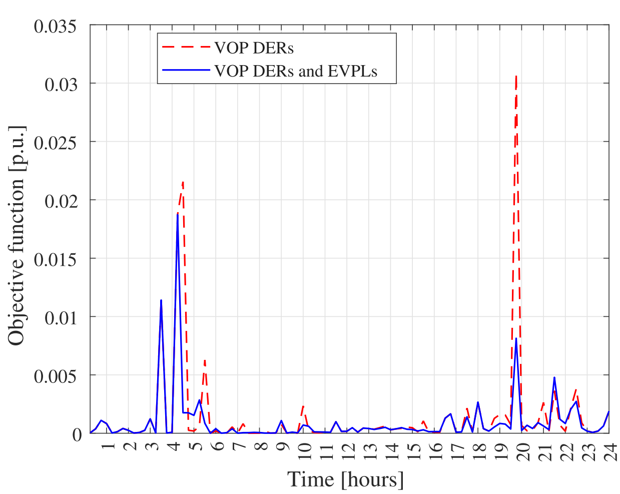

Fig. 15. Objective function of Case B.

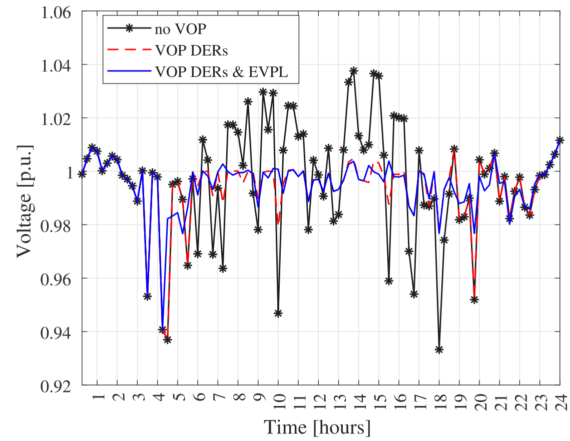

Fig. 16. PN_3 voltage profiles during the 24 h in Case B.

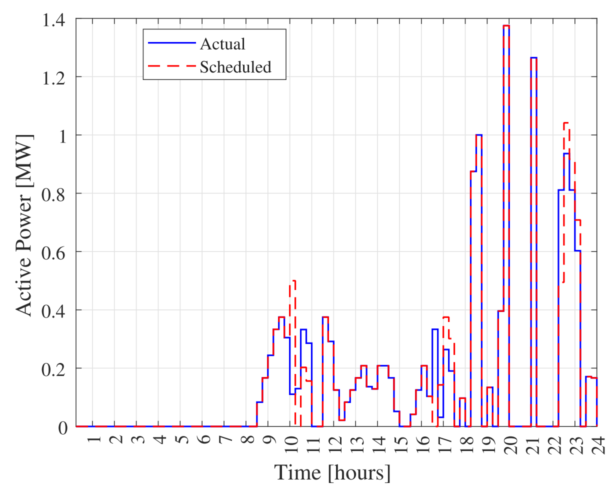

Fig. 17. PL_1 scheduled (reference) vs. optimized consumption profiles in Case B.

Figs. 17–20 show the time evolution of the active power absorbed by $EVPL_1$–$EVPL_4$ in Case B. In particular, the scheduled absorption is compared with the actual value obtained using the *VOP DERs and PLs* algorithm. The curves show the recovery effect after each period in which the proposed algorithm changes the actual PL power consumption from the reference value. Compared to Case A, in Case B, there are more periods when the flexibility of the PLs is exploited with an absorption increase (and consequent decrease during the following three recovery periods). In fact, there are more periods characterized by significant voltage increase beyond the rated value, as shown by the black profile in Fig. 16. Regarding the total daily energy absorbed by the PLs, the results are the same as in Case A and are reported in Table 7, as there is no difference in the models adopted for the four PLs in both cases.

4.2.3. Cost analysis

This subsection focuses on the economic aspects of using the flexibility provided by PLs. Constraint (35) limits the cost of the service purchased by the DSO. The unitary price of the flexibility provided by the PLs related to cost function c_{pl} in (30) was fixed at 25 €/MWh for both upstream and downstream power variations, which is a portion of the total price for the service provided by the PLs to the DSO, referred to as the effective use of flexibility during the operation. The limit b^t_{DSO} of the budget available to the DSO is set to 50 €/h for all t. Under these assumptions, the Total Daily Cost (TDC) of the PL flexibility service used by the DSO was 99.7 €/day in Case A and 105.5 €/day in Case B. The difference between these values is due to the varying PV generation and system loading conditions in Cases A and B. Generally, these values

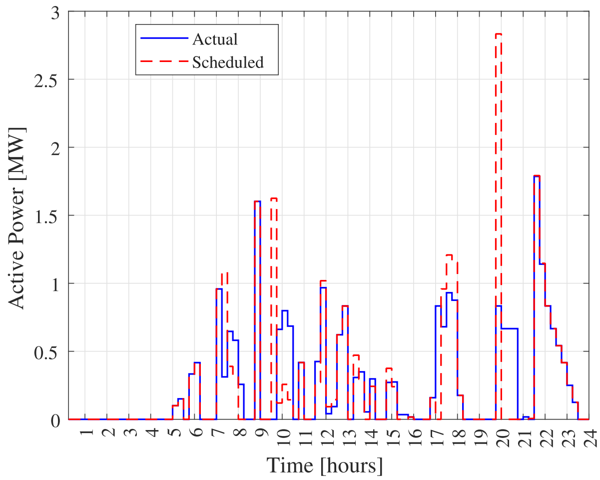

Fig. 18. PL_2 scheduled (reference) vs. optimized consumption profiles in Case B.

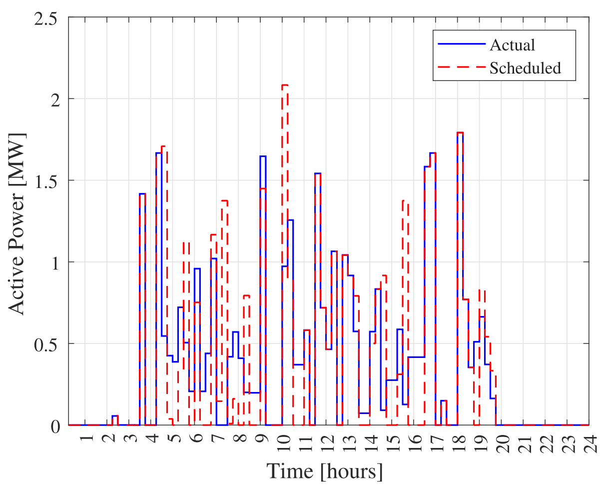

Fig. 19. PL_3 scheduled (reference) vs. optimized consumption profiles in Case B.

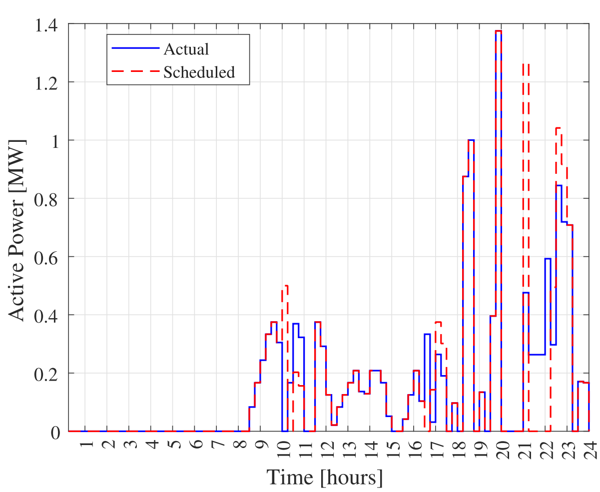

Fig. 20. PL_4 scheduled (reference) vs. optimized consumption profiles in Case B.

can be considered as the cost of optimizing the voltage profiles using PL flexibility.

Tables 8 and 9 show the variations of the VDI and of the TDC results when the budget available to the DSO is reduced, for Case A and Case B, respectively. As expected, VDI increased and TDC decreased as the budget limit decreased. For b^t_{DSO} = 1 €/h, the VDI is close to the values reported in Table 6 for the *VOP DERs* algorithm, which does not take advantage of PL flexibility.

Table 8
VDI and TDC for various values of the DSO budget b^t_{DSO} in Case A.

	b^t_{DSO} (€/h)				
	50	25	10	5	1
VDI (p.u.)	0.101	0.109	0.124	0.137	0.150
TDC (€/day)	99.7	88.5	57.9	30.6	6.5

Table 9
VDI and TDC for various values of the DSO budget b^t_{DSO} in Case B.

	b^t_{DSO} (€/h)				
	50	25	10	5	1
VDI (p.u.)	0.091	0.100	0.115	0.126	0.138
TDC (€/day)	105.5	85.2	50.7	29.2	5.8

5. Conclusion

This paper presents a method to assess the maximum level of consumption flexibility that an EV parking lot can offer to the DSO while still ensuring proper EV charging services. This flexibility, along with that of the other DERs, is used for real-time voltage profile optimization.

Regarding the calculation approach for parking lot flexibility, the reference consumption profiles and the maximum allowable active power flexibility adjustments for each 15-min interval throughout the day are determined using stochastic linear optimization.

The DSO voltage optimization procedure employs a multiperiod model to adequately account for energy recovery effects over subsequent time intervals. By ensuring full recovery of the energy required by the parking lots, the VOP uses flexibility without compromising the quality of the EV charging services. The VOP model decomposes the network into voltage control zones and uses a linearized power flow model.

Numerical tests were conducted considering four parking lots and 15 DERs connected to the IEEE 123 node test feeder over a 24-h period. Two cases were considered, referred to as Case A and Case B, based on the rated power of each PV system, which is assumed to be equal to 200 kW for Case A and 300 kW for Case B. Cases A and B also differs with respect to the system loading conditions: in Case B, the total daily load curve was reduced to 30% of that of Case A.

For the considered cases, the voltage profiles are obtained using three different approaches: power flow calculation without voltage optimization (*no VOP*), voltage optimization performed by adjusting only the DER reactive outputs (*VOP DERs*), and voltage optimization performed by adjusting both the DER reactive power and active power absorption of the parking lots (*VOP DERs and PLs*).

The results are compared in terms of the voltage deviation index, actual power absorbed by the parking lots during the day with respect to the reference consumption profile, and total daily energy consumed by the parking lots. In addition, a sensitivity analysis was conducted on the impact of the assumed cost of flexibility provided by the EV parking lots.

The results shows that the use of parking lot flexibility allows significant voltage deviation reductions compared to both cases without voltage optimization and voltage optimization that varies only DER reactive powers. In particular, the solution of the *VOP DERs and PLs* algorithm improves the voltage deviation index by approximately 70% and 75% for Cases A and B, respectively, compared with that of the *no VOP* algorithm; the improvements are approximately 34% for Case A and 35% for Case B if compared with the solution of the *VOP DERs* algorithm.

Furthermore, this procedure guarantees complete energy recovery for the EV charging service during 24 h of the day, and the computational effort required for the voltage optimization procedure is compatible with online applications.

The study also quantified the total daily costs associated with the use of parking lot flexibility for voltage profile optimization, focusing on the impact of the reduced DSO budget on the voltage deviation from the rated value.

The results indicate that the proposed algorithm is particularly effective when the DER production levels are high and closely align with parking lot consumption.

The aspects of the proposed method that deserve further improvements are primarily related to the need of a more accurate representation of the distribution network in presence of unbalanced operating conditions. The VOP model can be extended to account for the uncertainties related to other sources of flexibility beyond parking lots. Moreover, further services could be considered from the DSO point of view in addition to voltage profile optimization, such as congestion management. Finally, future work will also focus on the use of decomposition approaches to allow a fast solution to the voltage optimization problem, even for very large test cases.

CRediT authorship contribution statement

Michele De Santis: Writing – review & editing, Writing – original draft, Visualization, Validation, Supervision, Software, Resources, Project administration, Methodology, Investigation, Funding acquisition, Formal analysis, Data curation, Conceptualization. **Tohid Harighi:** Writing – review & editing, Writing – original draft, Visualization, Validation, Supervision, Software, Resources, Project administration, Methodology, Investigation, Funding acquisition, Formal analysis, Data curation, Conceptualization. **Anna Rita Di Fazio:** Writing – review & editing, Writing – original draft, Visualization, Validation, Supervision, Software, Resources, Project administration, Methodology, Investigation, Funding acquisition, Formal analysis, Data curation, Conceptualization. **Alberto Borghetti:** Writing – original draft, Visualization, Validation, Supervision, Software, Resources, Project administration, Methodology, Investigation, Funding acquisition, Formal analysis, Data curation, Conceptualization. **Mario Russo:** Writing – review & editing, Writing – original draft, Visualization, Validation, Supervision, Software, Resources, Project administration, Methodology, Investigation, Funding acquisition, Formal analysis, Data curation, Conceptualization.

Research ethics

We further confirm that the work covered in this manuscript has not involved human patients.

Funding

No funding was received for this work.

Declaration of competing interest

No conflict of interest exists.

We wish to confirm that there are no known conflicts of interest associated with this publication and there has been no significant financial support for this work that could have influenced its outcome.

Acknowledgments

This paper is an extended version of the paper "Flexible operation of an EV parking lot for voltage control of a distribution network" [34], which was presented at the 2023 International Conference on Smart Energy Systems and Technologies (SEST), Mugla, Turkey, in Sept. 2023. The authors would like to thank the participants for the useful discussions at the presentation.

Data availability

Data will be made available on request.

References

[1] Hannu Laaksonen, Hosna Khajeh, Chethan Parthasarathy, Miadreza Shafie-khah, Nikos Hatziargyriou, Towards flexible distribution systems: Future adaptive management schemes, Appl. Sci. 11 (8) (2021) http://dx.doi.org/10.3390/app11083709, URL https://www.mdpi.com/2076-3417/11/8/3709.

[2] Anamika Dubey, Sumit Paudyal, Distribution system optimization to manage distributed energy resources (DERs) for grid services, Found. Trends® Electr. Energy Syst. 6 (3–4) (2023) 120–264, http://dx.doi.org/10.1561/3100000030.

[3] M.R.M. Cruz, Desta Z. Fitiwi, Sérgio F. Santos, João P.S. Catalão, A comprehensive survey of flexibility options for supporting the low-carbon energy future, Renew. Sustain. Energy Rev. 97 (2018) 338–353.

[4] Giuditta Pisano, Simona Ruggeri, Gian Giuseppe Soma, Davide Falabretti, Samuele Grillo, Francesco Gulotta, Fabrizio Pilo, Impact of electrical vehicle private charging stations on the quality of the low voltage network supply, IEEE Open Access J. Power Energy 10 (2023) 351–362, http://dx.doi.org/10.1109/OAJPE.2023.3258254.

[5] R. Khan, K.K. Mehmood, S.B.A. Bukhari, K. Imran, A. Wadood, S.B. Rhee, S. Park, An optimization-based reliability enhancement scheme for active distribution systems utilizing electric vehicles, IEEE Access 9 (2021) 157247–157258, http://dx.doi.org/10.1109/ACCESS.2021.3127802.

[6] Wojciech Lewicki, Hasan Huseyin Coban, Jacek Wróbel, Integration of electric vehicle power supply systems—Case study analysis of the impact on a selected urban network in Türkiye, Energies 17 (14) (2024) http://dx.doi.org/10.3390/en17143596.

[7] Nataly Bañol Arias, Seyedmostafa Hashemi, Peter Bach Andersen, Chresten Træholt, Rubén Romero, Distribution system services provided by electric vehicles: Recent status, challenges, and future prospects, IEEE Trans. Intell. Transp. Syst. 20 (12) (2019) 4277–4296, http://dx.doi.org/10.1109/TITS.2018.2889439.

[8] Z. Wang, S. Wang, Grid power peak shaving and valley filling using vehicle-to-grid systems, IEEE Trans. Power Deliv. 28 (3) (2013) 1822–1829, http://dx.doi.org/10.1109/TPWRD.2013.2264497.

[9] Magnus Korpås, Aurora F. Flataker, Hanne Sæle, Bendik Nybakk Torsæter, Karen Byskov Lindberg, Shanshan Jiang, Ase Lekang Sørensen, Audun Botterud, Learning from the norwegian electric vehicle success: An overview, IEEE Power Energy Mag. 21 (6) (2023) 18–27, http://dx.doi.org/10.1109/MPE.2023.3308246.

[10] F. Marasciuolo, C. Orozco, M. Dicorato, A. Borghetti, G. Forte, Chance-constrained calculation of the reserve service provided by EV charging station clusters in energy communities, IEEE Trans. Ind. Appl. 59 (4) (2023) 4700–4709, http://dx.doi.org/10.1109/TIA.2023.3264965.

[11] Stylianos I. Vagropoulos, Pandelis N. Biskas, Anastasios G. Bakirtzis, Market-based TSO-DSO coordination for enhanced flexibility services provision, Electr. Power Syst. Res. 208 (2022) 107883, http://dx.doi.org/10.1016/j.epsr.2022.107883.

[12] Y. Li, M. Han, Z. Yang, G. Li, Coordinating flexible demand response and renewable uncertainties for scheduling of community integrated energy systems with an electric vehicle charging station: A Bi-level approach, IEEE Trans. Sustain. Energy 12 (2021) 2321–2331.

[13] K. Ma, X. Hu, Z. Yue, Y. Wang, J. Yang, H. Zhao, Z. Liu, Voltage regulation with electric taxi based on dynamic game strategy, IEEE Trans. Veh. Technol. 71 (3) (2022) 2413–2426, http://dx.doi.org/10.1109/TVT.2022.3141954.

[14] Harshavardhan Patil, Vaiju Nago Kalkhambkar, Grid integration of electric vehicles for economic benefits: A review, J. Mod. Power Syst. Clean Energy 9 (1) (2021) 13–26, http://dx.doi.org/10.35833/MPCE.2019.000326.

[15] Miadreza Shafie-Khah, Pierluigi Siano, Desta Z. Fitiwi, Nadali Mahmoudi, João P.S. Catalão, An innovative two-level model for electric vehicle parking lots in distribution systems with renewable energy, IEEE Trans. Smart Grid 9 (2) (2018) 1506–1520, http://dx.doi.org/10.1109/TSG.2017.2715259.

[16] S. Muhammad Bagher Sadati, Jamal Moshtagh, Miadreza Shafie-khah, Abdollah Rastgou, João P.S. Catalão, Operational scheduling of a smart distribution system considering electric vehicles parking lot: A bi-level approach, Int. J. Electr. Power Energy Syst. 105 (2019) 159–178, http://dx.doi.org/10.1016/j.ijepes.2018.08.021, URL https://www.sciencedirect.com/science/article/pii/S0142061518304824.

[17] Xi Lu, Ka Wing Chan, Shiwei Xia, Mohammad Shahidehpour, Wing Ho Ng, An operation model for distribution companies using the flexibility of electric vehicle aggregators, IEEE Trans. Smart Grid 12 (2) (2021) 1507–1518, http://dx.doi.org/10.1109/TSG.2020.3037053.

[18] Yahya Kabiri-Renani, Ali Arjomandi-Nezhad, Mahmud Fotuhi-Firuzabad, Mohammad Shahidehpour, Transactive-based day-ahead electric vehicles charging scheduling, IEEE Trans. Transp. Electr. (2023) http://dx.doi.org/10.1109/TTE.2023.3348490, 1–1.

[19] Sahand Karimi-Arpanahi, Mohammad Jooshaki, S. Ali Pourmousavi, Matti Lehtonen, Leveraging the flexibility of electric vehicle parking lots in distribution networks with high renewable penetration, Int. J. Electr. Power Energy Syst. 142 (2022) 108366, http://dx.doi.org/10.1016/j.ijepes.2022.108366.

[20] Hiroshi Kikusato, Ryu Ando, Jun Hashimoto, Kenji Otani, Nanae Kaneko, Optimal short-term charge/discharge operation for electric vehicles with volt-var control in day-ahead electricity market, IEEE Open Access J. Power Energy 11 (2024) 410–420, http://dx.doi.org/10.1109/OAJPE.2024.3444748.

[21] Md Murshadul Hoque, Mohsen Khorasany, Reza Razzaghi, Hao Wang, Mahdi Jalili, Transactive coordination of electric vehicles with voltage control in distribution networks, IEEE Trans. Sustain. Energy 13 (1) (2022) 391–402, http://dx.doi.org/10.1109/TSTE.2021.3113614.

[22] Md Murshadul Hoque, Mohsen Khorasany, Reza Razzaghi, Hao Wang, Mahdi Jalili, Hao Wang, Network-aware coordination of aggregated electric vehicles considering charge–discharge flexibility, IEEE Trans. Smart Grid 14 (3) (2023) 2125–2139, http://dx.doi.org/10.1109/TSG.2022.3204761.

[23] Kratika Yadav, Mukesh Singh, Dynamic scheduling of electricity demand for decentralized EV charging systems, Sustain. Energy Grids Netw. 39 (2024) 101467, http://dx.doi.org/10.1016/j.segan.2024.101467.

[24] Y. Zhou, F. Gao, Z. Zhang, S. Zhao, X. Xu, H. Meng, H. Gao, Research on optimal voltage control of distribution network with the participation of EVs and PVs, Appl. Sci. 13 (10) (2023) http://dx.doi.org/10.3390/app13105987, URL https://www.mdpi.com/2076-3417/13/10/5987.

[25] L. Cheng, Y. Chang, R. Huang, Mitigating voltage problem in distribution system with distributed solar generation using electric vehicles, IEEE Trans. Sustain. Energy 6 (4) (2015) 1475–1484, http://dx.doi.org/10.1109/TSTE.2015.2444390.

[26] B. Xu, G. Zhang, K. Li, B. Li, H. Chi, Y. Yao, Z. Fan, Reactive power optimization of a distribution network with high-penetration of wind and solar renewable energy and electric vehicles, Prot. Control Mod. Power Syst. 7 (51) (2022) 1–13, http://dx.doi.org/10.1186/s41601-022-00271-w.

[27] Alireza Kashki, Azita Azarfar, Mahmoud Samiei Moghaddam, Reza Davarzani, Optimal charging of electric vehicles in smart stations and its effects on the distribution network using meerkat optimization algorithm, Energy Rep. 12 (2024) 1936–1946, http://dx.doi.org/10.1016/j.egyr.2024.08.005.

[28] Renbo Wu, Shuqin Liu, Multi-objective optimization for distribution network reconfiguration with reactive power optimization of new energy and EVs, IEEE Access 11 (2023) 10664–10674, http://dx.doi.org/10.1109/ACCESS.2023.3241228.

[29] K. Ramakrishna, C.H. Hussaian, V. Prashanth, C. Dhanamjayulu, S. Sujata, R. Likhitha, A novel on energy management strategy with maximum exploitation of renewables and EV storage in distribution networks, Int. Trans. Electr. Energy Syst. (2023) 18, http://dx.doi.org/10.1155/2023/1365608.

[30] Ding Liu, Peng Zeng, Shijie Cui, Chunhe Song, Deep reinforcement learning for charging scheduling of electric vehicles considering distribution network voltage stability, Sensors 23 (3) (2023) http://dx.doi.org/10.3390/s23031618, URL https://www.mdpi.com/1424-8220/23/3/1618.

[31] F. Varshosaz, M. Moazzami, B. Fani, P. Siano, Day-ahead capacity estimation and power management of a charging station based on queuing theory, IEEE Trans. Ind. Inform. 15 (10) (2019) 5561–5574.

[32] A.R. Di Fazio, M. Russo, S. Valeri, M. De Santis, Linear method for steady-state analysis of radial distribution systems, Int. J. Electr. Power Energy Syst. 99 (2018) 744–755, http://dx.doi.org/10.1016/j.ijepes.2018.02.001.

[33] A.R. Di Fazio, C. Risi, M. Russo, M. De Santis, Coordinated optimization for zone-based voltage control in distribution grids, IEEE Trans. Ind. Appl. 58 (1) (2022) 173–184, http://dx.doi.org/10.1109/TIA.2021.3129731.

[34] T. Harighi, A. Borghetti, M. De Santis, A.R. Di Fazio, M. Russo, Flexible operation of an EV parking lot for voltage control of a distribution network, in: 2023 International Conference on Smart Energy Systems and Technologies, SEST, 2023, pp. 1–6, http://dx.doi.org/10.1109/SEST57387.2023.10257434.

[35] M.P. Evans, S.H. Tindemans, D. Angeli, Flexibility framework with recovery guarantees for aggregated energy storage devices, IEEE Trans. Smart Grid 13 (5) (2022) 3519–3531, http://dx.doi.org/10.1109/TSG.2022.3173900.

[36] C. Orozco, A. Borghetti, F. Napolitano, F. Tossani, Day-ahead multistage stochastic optimization of a group of electric vehicle charging stations, in: In Proc. IEEE CPE-POWERENG, Florence, Italy, 2021, pp. 1–6, http://dx.doi.org/10.1109/CPE-POWERENG50821.2021.9501228.

[37] Tohid Harighi, Alberto Borghetti, Fabio Napolitano, Fabio Tossani, Flexibility modeling for parking lots with multiple EV charging stations, Electr. Power Syst. Res. 234 (2024) 110732, http://dx.doi.org/10.1016/j.epsr.2024.110732.

[38] Anna Rita Di Fazio, Mario Russo, Michele De Santis, Zoning evaluation for voltage optimization in distribution networks with distributed energy resources, Energies 12 (3) (2019) 390, http://dx.doi.org/10.3390/en12030390.

[39] IEEE Distribution System Subcommittee, IEEE 123 Node Test Feeder, IEEE PES, 1992, https://cmte.ieee.org/pes-testfeeders/resources/.

[40] A.R. Di Fazio, M. Russo, M. De Santis, Zoning evaluation for voltage control in smart distribution networks, in: 18Th IEEE International Conference on Environment and Electrical Engineering, EEEIC June 2018, 2018, pp. 1–6, http://dx.doi.org/10.1109/EEEIC.2018.8493761.

[41] Ray Daniel Zimmerman, Carlos Edmundo Murillo-Sánchez, Robert John, Matpower: Steady-state operations, planning, and analysis tools for power systems research and education, IEEE Trans. Power Syst. 26 (1) (2011) 12–19, http://dx.doi.org/10.1109/TPWRS.2010.2051168.